

Milky Way Disk

Daisuke Kawata^{a,b}, Robert J.J. Grand^c, Jason A.S. Hunt^d and Ioana Ciucă^e

^aMullard Space Science Laboratory, University College London, Holmbury St. Mary, Dorking, Surrey RH5 6NT, UK

^bNational Astronomical Observatory of Japan, 2-21-1 Osawa, Mitaka, Tokyo 181-8588, Japan

^cAstrophysics Research Institute, Liverpool John Moores University, 146 Brownlow Hill, Liverpool L3 5RF, UK

^dSchool of Mathematics & Physics, University of Surrey, Guildford GU2 7XH, UK

^eKavli Institute for Particle Astrophysics & Cosmology (KIPAC), Stanford University, Stanford, CA 94305, USA

© 20xx Elsevier Ltd. All rights reserved.

Chapter Article tagline: update of previous edition,, reprint..

Glossary

α -elements Elements, such as O, Mg, S, Si, Ca, and Ti, whose atomic mass number is a multiple of the mass number of ⁴He, whose nucleus is called α -particle.

[α /Fe] Abundance ratio between α -element and iron with respect to that for the Sun in log scale.

Apo-center The largest galactocentric radius in an orbit of the star.

Astrophysical stellar parameters Stellar effective temperature, T_{eff} , gravity, $\log g$, metallicity, [M/H], and abundances of various elements.

Asymmetric drift The difference between the circular speed and the mean rotation velocity of the stars.

Co-rotation Resonance The condition where the orbital rotation frequency of the star matches that of the non-axisymmetric structure, such as a bar.

Galactic bar The bar-like stellar over-density structure in the inner galactic disk.

Chemically-defined thick and thin disks The old high-[α /Fe] thick stellar disk and the young low-[α /Fe] thin stellar disk.

Circular orbit The orbit of an object along a complete circle, no radial motion, in the galactic disk.

Circular speed The rotation speed of the object in a circular orbit.

Cosmological simulation Computer numerical simulation, self-consistently following the formation of the large-scale structure and the formation of the galaxies under an assumed cosmology.

Dynamically self-consistent Kinematics of stars is consistent with what is expected from the gravitational potential due to their own mass distribution.

Epicycle frequency Frequency of the radial oscillation of the stellar orbit.

Galactoseismology Studying the kinematic sub-structures of the Milky Way stellar disk and understanding the nature of the Milky Way disk from their dynamical response to perturbations.

Geometrically-defined thick and thin disk Geometrically thick and thin stellar disk components.

Local Standard of Rest (LSR) A point rotating with a circular speed at the Galactocentric radius of the Sun.

Moving group A group of stars sharing a similar position and motion in the phase space. The classical ones are the groups of stars identified in the radial and rotation velocity distribution of the solar neighborhood stars.

Pattern speed Angular speed of a non-axisymmetric feature rotating in the galactic disk.

Peri-center The smallest galactocentric radius in an orbit of the star.

Phase space Six dimensional space of the position and velocity of stars.

Phase spiral Spiral arm feature observed in a position and velocity map, such as the vertical position and velocity map, of the stars.

Proper motion The angular change in the position of the celestial object in the sky over the time.

Proper motion of the Sun The offset velocity of the Sun from the LSR at the Galactocentric radius of the Sun.

Radial migration The change in the angular momentum of the disk stars.

Orbital Resonance The condition where orbital epicycle frequency is a simple multiple of the difference in the rotation frequencies of the star and that of the non-axisymmetric structure, such as a bar.

Rigid-body rotation A feature in the galactic disk rotating at a same angular speed at different radii, so that the shape of the feature does not change in time.

Rotation curve The circular speed as a function of the galactocentric radius.

Spiral arms The spiral-like structure of the over-density of stars and gas in the galactic disk.

Stellar astrometry Measurements of the position, including parallax, and motion of the stars.

Stellar parallax The apparent angle difference in the stellar position when observed from the Earth and from the Sun, which provides the distance of the star by trigonometry.

Nomenclature

BPX-bulge	Boxy/Peanut/X-shape-bulge
GSE	Gaia-Sausage-Enceladus
GGS	Great Galactic Starburst
ILR	Inner Lindblad Resonance
LSR	Local Standard of Rest
OLR	Outer Lindblad Resonance
SNe II	Type II supernovae
SNe Ia	Type-Ia supernovae

Abstract

Our understanding of the Milky Way disk is rapidly improving with the recent advent of the high quality and vast amount of observational data. We summarize our current view of the structure of the Milky Way disk, such as the masses and sizes of the gas and stellar disks, and the position and motion of the Sun in the disk. We also discuss the different definitions of the thick and thin disks of the Milky Way, the non-axisymmetric structures of the stellar disk, such as the bar and spiral arms, and the radial migration which can be triggered by these non-axisymmetric stellar structures. After the revolutionary data from the European Space Agency's Gaia mission, our view of the Milky Way disk has been transformed to a non-equilibrium system with many complicated structures in stellar kinematic distribution. We also summarize the recent findings of Galactoseismology research. These detailed observational data provide the archaeological information for us to unveil the formation and evolution history of the Milky Way disk, with the aid of the high-resolution numerical simulations of the Milky Way-like galaxy formation. We also discuss the current view of the formation history of the Milky Way disk.

Key Points

- The Milky Way is a barred spiral disk galaxy. The Milky Way disk has a stellar bar in the inner disk, and also has spiral arms. The number and shape of the spiral arms are still unknown.
- The Milky Way disk consists of the gas and stellar disks. The stellar disk shows the geometrically thick and thin disks. Also, there are two distinct stellar populations with different chemical abundances, high and low $[\alpha/\text{Fe}]$ abundances, corresponding to thick and thin disks, respectively. These geometrically-defined thick and thin disks are not same as the chemically-defined thick and thin disks.
- The Milky Way disk is not completely in dynamically equilibrium. There are many kinematic sub-structures, such as ridges and corrugation features, observed. The outer disk shows the upward and down-ward warps in the opposite sides of the disk.
- The main source of the perturbation is considered to be the Sagittarius dwarf galaxy, which is falling into the Milky Way. However, the exact mechanism causing the observed stellar kinematic features are still in debate.
- The Milky Way disk formation likely started with gas-rich mergers at the early epoch of the Universe, which built the thick disk. Then, following a long term quiet phase of no significant merger helped to build the thin disk. The last most significant merger, the Gaia-Sausage-Enceladus merger, likely impacted the transition from the thick disk to the thin disk formation phase.

1 Introduction

One of the most striking and fascinating features visible in the night sky is the stream of stars overarching the sky. This is merely an edge-on view of the stellar disk of our Galaxy, and from this view the name of the Milky Way derives. Thus, understanding the structure of the Milky Way disk and its formation history has been a fundamental topic of astronomy since ancient times.

Our understanding of the Galactic disk has been dramatically enhanced due to the advent of ground-based and space-based observational facilities covering all the wavelengths of light from the gas and stars, and powerful computing facilities. In particular, the European Space Agency (ESA)'s Gaia mission (Gaia Collaboration et al., 2016) has revolutionized our view of the Milky Way disk. The Gaia mission launched in 2013 is the successor to ESA's Hipparcos mission (1989–1983) which was the first space astrometry mission, and measured parallaxes and proper motions for approximately 118,000 bright stars. The sharp image of stars obtained in space allows space missions to precisely measure the stars' positions in the sky. The positions of these stars in the sky vary with the Earth's orbit around the Sun, and the magnitude of these differences for a given star, otherwise known as the trigonometric parallax angle, gives the distance to the star. In addition, the long time baseline of the observations allows the measurement of the movement of stars, i.e. the proper motion of the stars. Although the final data release of the Gaia mission is planned in the 2030s, the Gaia mission has made several intermediate data releases already. Their 3rd data release (Gaia DR3) provides the precise positions, parallaxes, and proper motions for about 1.5 billion stars up to $G \sim 21$ mag with about 100 times better accuracy than what was achieved by Hipparcos. In addition, the radial velocities measured with the onboard spectrograph, RVS, provide radial velocities for about 33 million stars brighter than $G_{\text{RVS}} \sim 14$ mag. Astrophysical parameters of stars, such as effective temperature, T_{eff} , gravity, $\log g$, metallicity, $[\text{M}/\text{H}]$, and abundances of various elements are also measured with the RVS spectra and the onboard BP/RP spectro-photometric data.

Spectroscopic stellar surveys, such as the RAdial Velocity Experiment (RAVE), the Sloan Digital Sky Survey (SDSS), the Sloan Extension for Galactic Understanding and Exploration (SEGUE), the Apache Point Observatory Galactic Evolution Experiment (APOGEE), the Large Sky Area Multi-Object Fiber Spectroscopic Telescope (LAMOST), the Gaia-ESO survey, the Galactic Archaeology with HERMES

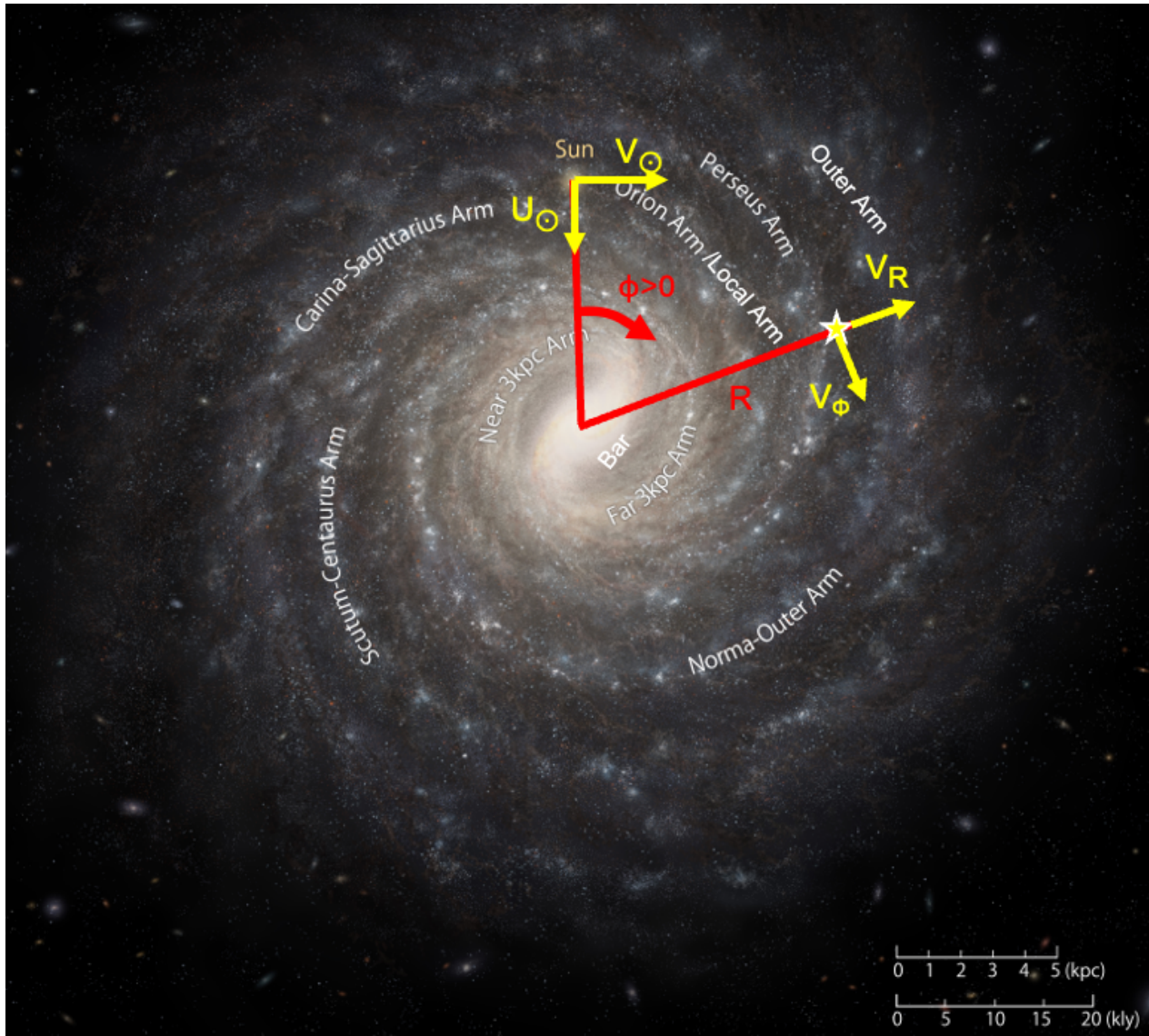


Fig. 1 Artist impression of the Milky Way disk in the face-on view. In this view, the Milky Way disk is rotating clockwise. The arrows from the Sun indicate the directions of the Sun's radial, U_{\odot} , and azimuthal, V_{\odot} , proper motion. The yellow star symbol presents an example star. The yellow arrows from the star show the directions of their radial, V_R , and azimuthal, V_{ϕ} , velocities. The red line from the center of the Milky Way to the star indicates the Galactocentric radius of the star, R . The red line from the center to the Sun is where the azimuthal angle, $\phi = 0$. The red arrow shows the direction of the positive ϕ . The bar and the name of the spiral arms are also highlighted. Modified from NAOJ, Nakanishi and Sofue (2016), Reid et al. (2019), and Baba et al. (2022).

survey (GALAH), and HectoChelle in the Halo at High Resolution survey (H3) are adding value to the Gaia data by providing further, more detailed chemical abundance information for a portion of the Gaia stars. In addition, the cold gas, including dust and molecular gas, neutral hydrogen gas, and the warm and hot gas distribution in the Milky Way are revealed by the X-ray to radio observations. These observational data are compared with theoretical models and our understanding of the current structure and formation history of the Milky Way disk has significantly improved recently.

This chapter summarizes our current understanding of the Milky Way disk. Section 2 describes the overall structure of the Milky Way disk unveiled by the Gaia mission. Section 3 shows the current view of the formation process of the Milky Way disk. Section 4 provides the summary of the chapter and future prospects.

2 The structure of the Milky Way Disk

Figure 1 shows an artist's impression of the overall structure of the Milky Way disk as viewed face-on. The Milky Way is believed to be a barred spiral disk galaxy. It is still challenging to capture the true structure of the whole Milky Way disk. This is because we live within the Milky Way disk, and it is impossible to see the whole Milky Way from outside. Although we can measure the position of individual stars in the Milky Way disk, accurately measuring the distance to the faint and/or distant stars is always a challenge in astronomy. In addition, the interstellar dust with complex structure blocks starlight in complicated ways. Therefore, it is not straightforward to obtain the true density distribution of the stars in the Milky Way disk. Still, our understanding of the structure of the Milky Way disk is rapidly improving with data from Gaia and other complementary Milky Way surveys.

In this section, we provide an overall picture of the Milky Way disk in our current view. The basic structure of the Milky Way is also summarized in Bland-Hawthorn and Gerhard (2016) and McMillan (2017). A thorough review of the stellar kinematics of the Milky Way is provided in Hunt and Vasiliev (2024). A comprehensive Milky Way stellar distribution model which describes all the disk, bulge and halo stars was constructed by Robin et al. (2003) and is known as the Besançon Galaxy Model¹. The Besançon Galaxy Model is regularly updated and the latest model (Robin et al., 2022), which includes the dark matter halo, is adjusted to match the Gaia data and is dynamically self-consistent: the kinematics of stars are consistent with what is expected from the gravitational potential due to their mass distribution. The model provides the mass and size of 8 different disks with different masses and ages: the oldest one corresponds to the thick disk (Section 2.2). The Besançon Galaxy Model is one of the valuable reference models of the whole Milky Way.

Section 2.1 summarizes the mass and size of the different components of the Milky Way disk. In Section 2.2, we describe the thick and thin disk stellar populations. Sections 2.3.1 and 2.3.2 describe the bar and spiral structures, respectively. Section 2.3.3 describes the radial migration process induced by the bar and spiral arm structures. Section 2.4 provides the current status of Galactoseismology, which studies how the Milky Way responds to past dynamical impacts through observed kinematic sub-structures in the Milky Way disk stars.

2.1 Mass and size of the Milky Way disk

2.1.1 Stellar disk

The overall stellar mass of the Milky Way disk is estimated to be about $M_{\star, \text{disk}} = 3 - 5 \times 10^{10} M_{\odot}$ (e.g., Licquia and Newman, 2016; Binney and Vasiliev, 2024). The surface mass density profile of the galactic disk is generally well described with an exponential profile,

$$\Sigma(R) = A \exp(-R/R_{d,\star}), \quad (1)$$

where $R_{d,\star}$ is the scale length of the disk and R is the Galactocentric radius in the cylindrical coordinate. Compiling the data from the literature, Licquia and Newman (2016) estimate $R_{d,\star} \sim 2.6$ kpc. However, the scale length of the Milky Way disk as defined in this way is much smaller compared to other disk galaxies of similar stellar mass to the Milky Way. Lian et al. (2024) argue that the radial density profile of the Milky Way depends on stellar age, and that they are not well-described with a single exponential profile, but are rather better explained with broken-exponential profiles. They obtain the half-light radius (the radius which contains half of the total disk starlight) to be $R_{50} = 5.75 \pm 0.38$ kpc, which is consistent with other external disk galaxies of similar mass to the Milky Way.

2.1.2 Gas disk

The Milky Way disk also contains a gas disk. Compiling the literature data, McMillan (2017) estimates the mass and size of the Milky Way gas disk. The author uses the following function to describe the mass distribution of H I gas and molecular gas disks in cylindrical coordinates.

$$\rho_g(R, z) = \frac{\Sigma_g}{4z_{d,g}} \exp\left(-\frac{R_m}{R} - \frac{R}{R_{d,g}}\right) \text{sech}^2(z/2z_{d,g}). \quad (2)$$

This is similar to the exponential profile (equation 1) with scale length $R_{d,g}$ in the outer disk, but the density declines with decreasing R in the inner disk with a peak at $R = \sqrt{R_m R_{d,g}}$. The vertical density profile is described with sech^2 function with the scale height of $z_{d,g}$. McMillan (2017) suggests that the mass of HI disk is $M_{\text{HI}} = 1.1 \times 10^{10} M_{\odot}$ with the parameters of $R_{d,\text{HI}} = 7$ kpc, $R_{m,\text{HI}} = 4$ kpc, and $z_{d,\text{HI}} = 0.085$ kpc, and the mass of molecular gas disk is $M_{\text{H}_2} = 1.2 \times 10^{10} M_{\odot}$ with the parameters of $R_{d,\text{H}_2} = 1.5$ kpc, $R_{m,\text{H}_2} = 12$ kpc, and $z_{d,\text{H}_2} = 0.045$ kpc.

2.1.3 Sun's location and motion in the Milky Way disk

The Sun is located near the edge of the Milky Way disk, as shown in Figure 1. The distance to the Sun from the Galactic center, $R_0 = 8.275 \pm 0.09_{\text{stat.}} \pm 0.33_{\text{sys.}}$ kpc, is accurately measured using 16 years of the orbital data of the star S2 around the supermassive black hole, Sagittarius A* (Sgr A*), at the center of the Milky Way by GRAVITY Collaboration et al. (2021). Here, $_{\text{sys.}}$ and $_{\text{stat.}}$ indicate systematic and statistical uncertainties, respectively. The systematic uncertainty is more difficult to assess than the statistical uncertainty. Unless otherwise stated, the uncertainties shown in this chapter indicate the latter.

Reid and Brunthaler (2020) measure the proper motion of the radio emission from Sgr A* with respect to two extra-galactic (therefore stationary) radio sources using 18 years of the Very Long Baseline Array data. They find negligible intrinsic motion of Sgr A*, i.e. the proper motion of Sgr A* is reflecting the motion of the Sun in the Milky Way.

¹<https://model.obs-besancon.fr/>

The Sun is rotating around the Milky Way disk at the Galactocentric radius of R_0 . The Sun's proper motion is defined as the offset of Sun's velocity from the Local Standard of Rest (LSR). The LSR is defined as a point rotating with a circular speed, Θ_0 , at R_0 , i.e. having a completely circular orbit without any radial motion. The radial, azimuthal, and vertical components of Solar motion with respect to LSR are denoted with U_\odot , V_\odot , and W_\odot , respectively (Figure 1). The above-mentioned proper motion of Sgr A* provides the Sun's total motion in the Galactic rest frame. Hence, the longitudinal proper motion of Sgr A* corresponds to the total rotation speed of the Sun, $\Theta_0 + V_\odot$. Using this and R_0 measured by GRAVITY Collaboration et al. (2021) as the strong priors, Almannæi et al. (2024) fit the kinematics of the young stars in the Gaia Data Release 3 (Gaia DR3, Gaia Collaboration et al., 2023) with an axisymmetric disk model. The young stars, such as O-type and B-type stars (OB stars), are expected to closely follow the circular motion. Hence, their asymmetric drift, the difference between the mean rotation velocity of the stars and the circular velocity, is very small, and they are an ideal tracer to measure the circular speed. Using the Gaia DR3 OB stars' data, Almannæi et al. (2024) obtain $\Theta_0 = 234 \pm 2 \text{ km s}^{-1}$, $\Theta_0 + V_\odot = 248 \pm 2 \text{ km s}^{-1}$, and $U_\odot = -9.65 \pm 0.43 \text{ km s}^{-1}$, which are consistent with the other studies. Comparing with the numerical simulations of a disk galaxy model with a bar and spiral arms, Almannæi et al. (2024) note that the stellar kinematics are affected by the non-axisymmetric structures, such as the bar and the spiral arms (see more information in Sections 2.3.1 and 2.3.2), and therefore it is challenging to accurately measure the circular speed of the Milky Way. However, they demonstrate that taking the stellar kinematics in a larger region, e.g. within 2 kpc of the Sun, mitigates the issue.

The proper motion of Sgr A* in the latitudinal direction reflects the Sun's motion toward the North Galactic pole, which is transformed to $W_\odot = 8.57 \pm 0.27 \text{ km s}^{-1}$. The Sun is located above the mid-plane of the Milky Way disk. From Gaia DR2 data, Bennett and Bovy (2019) measure the distance of the Sun from the Galactic mid-plane to be $z_0 = 20.8 \pm 0.3 \text{ pc}$.

2.1.4 Local dark matter density from the Milky Way disk kinematics

Another important component contributing to the gravitational potential in the Milky Way disk is dark matter. The stellar and gas kinematics follows the total gravitational potential of the star, gas, and dark matter. Analyses of the total density of the local volume and finding the missing mass density, comparing it with the visible mass density, date back to 1920s, such as Kapteyn (1922) and Jeans (1922). The reviews of the various methods using the modern data are found in Read (2014) and de Salas and Widmark (2021). de Salas and Widmark (2021) compiled the post-Gaia measurements of the local dark matter density and highlighted that the various measurements of the local dark matter density at the Solar position show a wide range of values $\rho_{\text{DM},\odot} = 0.008 - 0.016 \text{ M}_\odot \text{ pc}^{-3}$. The reason for the discrepancy between the methodologies is likely due to the required assumption of equilibrium of the disk kinematics. As discussed in Section 2.4, the Gaia data have uncovered the disequilibrium of the Milky Way disk, which inevitably impacts the accuracy of the measurements of the gravitational potential from the disk kinematics.

2.1.5 Rotation curve

The kinematics of the stars and gas of the Milky Way disk can provide the circular speed as a function of the Galactocentric radius, the so-called the rotation curve (Sofue, 2020). The mean rotation velocity of stars, $\langle v_\phi(R) \rangle$, is usually slower than the circular speed, $\Theta(R)$, and this difference is called asymmetric drift, as mentioned above. The amount of asymmetric drift depends on the radial velocity dispersion profile, $\sigma_R(R)$, and the density profile of the tracer stars, $\Sigma(R)$. Hence, to measure the rotation curve, we need to accurately measure both the density profile and kinematics of the tracer stars. Recent studies of measuring the Milky Way rotation curve based on the Gaia data and ground-based spectroscopic survey data reach up to about $R = 30 \text{ kpc}$. Interestingly, several studies (e.g., Wang et al., 2023) find a declining rotation curve at $R \gg 17 \text{ kpc}$. This indicates lower dark matter contribution than what is expected from the standard dark matter density profile for the Milky Way halo whose mass is around $M_{\text{tot}} = 10^{12} \text{ M}_\odot$ and inferred with the larger radii tracers, such as globular clusters and satellite galaxies (e.g., Wang et al., 2020; Hunt and Vasiliev, 2024, for a review). This tension remains a puzzling issue. However, we note that accurately obtaining the density profile, especially in the outer disk, is challenging, and studies use the extrapolation of an exponential profile, like equation (1), with the scale length and scale height inferred in the inner disk. Hence, more observational data in the outer disk would be crucial to resolve this tension.

2.2 Thick and Thin disks

From the vertical number density profile of stars, Yoshii (1982) and Gilmore and Reid (1983) found a separate, thicker disk component to the main stellar thin disk. This extra component is called the thick disk. Each of these stellar disk density distributions is described with an exponential profile in both radial and vertical directions as the following equation.

$$\Sigma_\star(R, z) = \frac{\Sigma_{0,\star}}{2z_{d,\star}} \exp\left(-\frac{R}{R_{d,\star}} - \frac{|z|}{z_{d,\star}}\right), \quad (3)$$

where $R_{d,\star}$ is called the scale length and $z_{d,\star}$ is called the scale height. Please note that the scale height in the exponential law is different from the scale height in sech^2 profile used for the gas density profile in equation (2). In this description, the total mass of the component can be conveniently described as $M_\star = 2\pi\Sigma_{0,\star}R_{d,\star}^2$. Analyzing the number counts of the stars using the photometric data of SDSS, Jurić et al. (2008) obtain $R_{d,\text{thick}} = 3.6 \text{ kpc}$ and $z_{d,\text{thick}} = 0.9 \text{ kpc}$ for the thick disk, while $R_{d,\text{thin}} = 2.6 \text{ kpc}$ and $z_{d,\text{thin}} = 0.3 \text{ kpc}$ for the thin disk. Following Kawata and Chiappini (2016), we call this definition of thick and thin disks "geometrically-defined" thick and thin disks.

On the other hand, the thick and thin disk stellar populations are often defined by their distinct chemical compositions. The most fundamental way of characterizing the chemical abundances of the stars is using the iron abundance with respect to the hydrogen abundance, $[\text{Fe}/\text{H}]$, and the α -element abundances with respect to the iron abundance, $[\alpha/\text{Fe}]$. Here, $[X/Y]$ means that the ratio of X and Y element

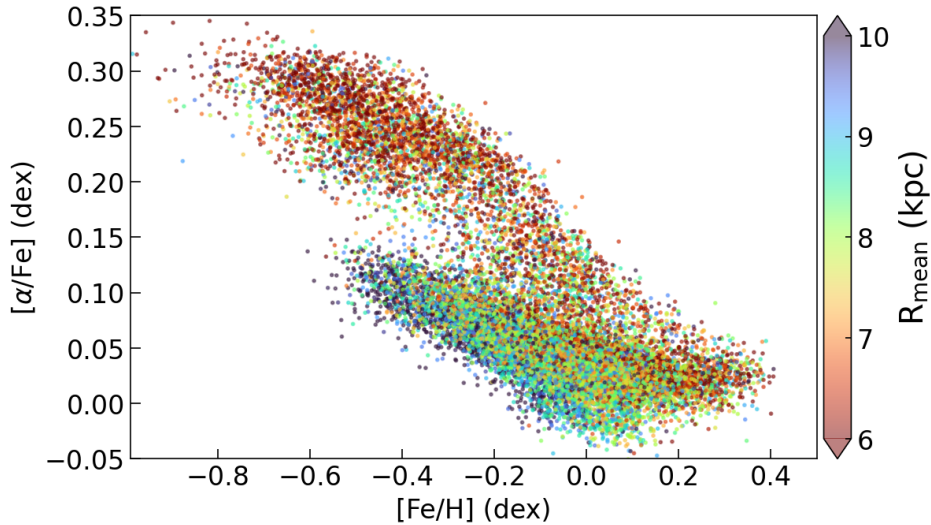


Fig. 2 [Fe/H] and $[\alpha/\text{Fe}]$ distribution of APOGEE giant stars in $R < 15$ kpc and $|z| < 3$ kpc color-coded with the mean orbital radius, R_{mean} .

abundance in log scale with respect to their abundance in the Sun, i.e.

$$[X/Y] = \log(Z_X/Z_Y)_\star - \log(Z_X/Z_Y)_\odot. \quad (4)$$

Here, Z_X means the mass fraction of X element with respect to the star's total mass. For example, for the Sun, the hydrogen abundance is $Z_{\text{H},\odot} = 0.7438$ (Asplund et al., 2021). α -elements include O, Mg, S, Si, Ca, and Ti, whose atomic mass number is a multiple of the mass number of ^4He , whose nucleus is called α -particle. The definition of α -element abundance often depends on the surveys, because different surveys use different spectrographs with different wavelength ranges and adopt different absorption lines and/or spectrum fitting methods to measure the abundance. For example in APOGEE DR17 (Majewski et al., 2017), α -abundance is a combination of the abundance of O, Mg, S, Si, Ca, and Ti, and the contribution from these different elements depends on the stellar parameters, such as effective temperature, T_{eff}^2 . Nevertheless, $[\alpha/\text{Fe}]$ is a good indicator of when stars were born. This is because α -elements are predominantly produced by Type II supernovae (SNe II) from massive ($m_\star > \sim 10 M_\odot$) stars whose lifetime is less than 10 Myr. On the other hand, Fe are more significantly produced by Type Ia SNe (SNe Ia), which may be from a merger of low-mass binary stars, whose lifetimes are in a wide range between 0.1 and 20 Gyr (e.g., Kobayashi et al., 2020). However, the exact progenitors of SNe Ia are still not well known. Consequently, stars are high- $[\alpha/\text{Fe}]$ abundance if they are born at a time when SNe II are dominant, i.e. during an active star formation phase. On the other hand, low- $[\alpha/\text{Fe}]$ stars can form when the star formation rate is decreasing or is at a lower level for a long time, because SNe Ia become more dominant than SNe II (e.g., Mason et al., 2024).

Figure 2 shows $[\text{Fe}/\text{H}]$ and $[\alpha/\text{Fe}]^3$ distribution of APOGEE DR17 giant stars from Ciucă et al. (2024)'s high-confidence age sample. As seen in Figure 2, high-resolution spectroscopic surveys of the Milky Way disk stars clearly show that there are two chemically distinct populations of stars, high- $[\alpha/\text{Fe}]$ and low- $[\alpha/\text{Fe}]$ populations in the large region of the Milky Way disk (e.g., Hayden et al., 2015; Imig et al., 2023). The high- $[\alpha/\text{Fe}]$ stars tend to have significantly higher velocity dispersion than the low- $[\alpha/\text{Fe}]$ stars (e.g., Sun et al., 2024). Hence, the high- $[\alpha/\text{Fe}]$ and low- $[\alpha/\text{Fe}]$ stars are also called thick and thin disks, respectively. Following Kawata and Chiappini (2016), we call these "chemically-defined" thick and thin disks. However, the chemically-defined thick and thin disks are not completely the same as the geometrically-defined thick and thin disks. For example, Bensby et al. (2014) show that the stars in the geometrically-defined thick disk are mainly in high- $[\alpha/\text{Fe}]$ population, but they are also spread in low- $[\alpha/\text{Fe}]$ population. Bovy et al. (2012) show that the high- $[\alpha/\text{Fe}]$ disk has a smaller scale length than the low- $[\alpha/\text{Fe}]$ disk. Figure 2 also shows that the high- $[\alpha/\text{Fe}]$ disk stars in the local disk tend to come from the inner disk, whose mean orbital radius, R_{mean} , is smaller. Here, R_{mean} is computed from the orbital integration under the Milky Way potential and defined as $0.5(R_{\text{apo}} + R_{\text{peri}})$, where R_{apo} and R_{peri} are the apo-center, the largest radius reached by the orbit of the star, and the peri-center, the smallest radius of the orbit. The orbits are computed with a galactic dynamics software package, `galpy`⁴ (Bovy, 2015), and the distance to the stars are taken from Queiroz et al. (2023). This is contradictory to the larger scale length of the geometrically-defined thick disk than the thin disk as mentioned above. Analyzing the numerical cosmological simulation result of a Milky Way-sized disk galaxy, Rahimi et al. (2014) find that this can be explained by the natural consequence of the cosmological formation history of galaxies. As we explain more in Section 3, the high- $[\alpha/\text{Fe}]$ disk forms at an early epoch as a thick and compact disk, while the low- $[\alpha/\text{Fe}]$ disk forms in the later phase as a thin and larger disk, but flaring (larger scale-height) at the outer radii. Hence, the low- $[\alpha/\text{Fe}]$ stars contribute to the geometrically thick

²<https://www.sdss4.org/dr17/irspec/parameters/>

³APOGEE DR17 provides $[\alpha/\text{M}]$ rather than $[\alpha/\text{Fe}]$, and "M" indicates the total metal abundance. However, to avoid a confusion, we call $[\alpha/\text{M}]$ in APOGEE data $[\alpha/\text{Fe}]$, since $[\text{Fe}/\text{H}]$ is very similar to $[\text{M}/\text{H}]$.

⁴<https://www.galpy.org/>

disk, and make the geometrically thick disk larger. In fact, Bensby et al. (2014) demonstrate that the chemically-defined thick and thin disks are more correlated with the age, and the chemically-defined thick disk is generally older than the chemically-defined thin disk. They also find that the high- $[\alpha/\text{Fe}]$ stars are more centrally concentrated than low- $[\alpha/\text{Fe}]$ stars. Although stellar ages are difficult to measure, Bensby et al. (2014) obtain the age for the turn-off stars and sub-giants using the stellar parameters, $\log g$, T_{eff} and $[\text{Fe}/\text{H}]$, precisely measured from high-resolution high signal-to-noise spectroscopic data. This age trend of the old chemically-defined thick and younger thin disks is also confirmed by the highly precise asteroseismology ages (e.g., Miglio et al., 2021a). Hence, it is better to define the two populations of the disks with age to associate with their formation history. However, since it is difficult to obtain the precise age for many stars, it is more convenient to define the distinct stellar populations of thick and thin disks using their chemical properties. Hereafter in this chapter, when we discuss the thick and thin disks, we indicate the chemically-defined old high- $[\alpha/\text{Fe}]$ thick disk and young low- $[\alpha/\text{Fe}]$ thin disk, respectively.

2.3 Bar and Spiral Arms

2.3.1 Bar

As shown in Figure 1, the Milky Way disk harbors a prominent bar structure in the inner disk region. However, the shape, angle, length, pattern speed, and formation time of the bar are all still in debate. The bar of the Milky Way was first suggested to explain the anomalous motion of the gas in the inner disk (Peters, 1975). The bar structure is also inferred from the asymmetry of the number of infrared bright stars (Nakada et al., 1991), and the near-infrared (NIR) emission distribution of the inner disk stars (Blitz and Spiegel, 1991).

Blitz and Spiegel (1991) note that the Cosmic Microwave Background Explorer (COBE) NIR image clearly shows the ‘‘peanut-shaped’’ bulge in the central region of the Milky Way disk. The red clump stars are in the core-helium burning phase of metal-rich stars with a specific absolute luminosity, and hence the red clump stars are often used as the standard candle to map the stellar structure of the Galactic disk. McWilliam and Zoccali (2010) find two groups of red clump stars at different distances in the inner bulge region, interpreting it as the X-shape of the inner bulge. Utilizing the large NIR photometric survey of the Galactic disk stars, VISTA Variables in the Via Lactea (VVV) survey, Wegg and Gerhard (2013) map the red clump stars’ density distribution, and reconstruct the clear Boxy/Peanut/X-shape (BPX) bulge structure. The major axis of the BPX-bulge extends up to about $R_{\text{BPX}} = 2$ kpc with the exponential scale length of each axes being (0.70, 0.44, 0.18) kpc along x_{BPX} , y_{BPX} , and z_{BPX} , where x_{BPX} is the major axis, and $x_{\text{BPX}} - y_{\text{BPX}}$ is in the disk plane. Because of the Peanut/X-shape, the vertical scale-height increases to 0.46 kpc at $x_{\text{BPX}} = 1.725$ kpc.

Although the connection between the BPX-bulge and the outer long bar was debated, analyzing the VVV data and using an N-body model as a prior, Wegg et al. (2015) convincingly show that the BPX-bulge is the inner region of the long bar, and the long bar extends to the radius of $R_{\text{lb}} = 5.0 \pm 0.2$ kpc. They also measure the angle of the bar from the line of the Sun and the Galactic center, and obtain the angle of $\phi_{\text{lb}} = 28^\circ - 33^\circ$. The long bar is also visible in the Gaia data combined with the APOGEE survey data (Queiroz et al., 2021). Also, Zhang et al. (2024) show that the bar is visible with the Gaia data’s low-amplitude long variable stars. They suggest that the bar length is about $R_{\text{lb}} = 4$ kpc, and obtain the bar angle of $\phi_{\text{lb}} = 25^\circ$ which is similar to Wegg et al. (2015). However, the end of the bar could overlap with the spiral arms, which affects the apparent size of the bar and the angle of the bar. Hence, the measurement and/or definition of the length of the bar and the angle of the bar are not straightforward to measure (e.g., Vislosky et al., 2024), and are still in debate.

Pattern speed of the bar

The stars in the bar region in the inner disk show a cylindrical rotation (e.g. Howard et al., 2008). This also means that the bar is a dominant structure in the inner disk, and the bar has a rigid-body rotation to keep its shape. Based on a comparison with a numerical simulation, Shen et al. (2010) estimate that the mass of the Milky Way bulge, i.e. nearly-spherical non-rotating stellar component, should be less than 8 % of the disk mass.

The pattern speed of the bar can be measured in several ways. The first convincing measurement was made by modelling the kinematics of the stars in the solar neighborhood. Several moving groups are identified in the radial and rotation velocity distribution of the stars in the solar neighborhood (Section 2.4). The Hercules stream is a prominent moving group, which shows slower rotation than the mean rotation speed of the other stars and moves outward in the Galactic disk. If the orbital angular frequency of Ω (the angular speed of stars in the azimuthal direction) and the epicyclic frequency, κ , are in relation with the pattern speed of the bar, Ω_{b} , as $\Omega_{\text{b}} = \Omega + \kappa/2$, which is called the Outer Lindblad Resonance (OLR), the orbit of the star has a closed ellipse orbit in the rotating frame of the bar. In this resonance orbit, a star completes exactly 2 radial oscillations, i.e. passing pericenter and apocenter twice for every rotation around the bar. Dehnen (1999) showed that Hercules stream could be caused by the bar’s OLR. If true, this would indicate the pattern speed of the bar to be about $\Omega_{\text{b}} = 53 \text{ km s}^{-1} \text{ kpc}^{-1}$. However, the Hercules stream can also be created by other resonances of the bar, including the co-rotation resonance, i.e. $\Omega_{\text{b}} = \Omega$, (Pérez-Villegas et al., 2017) and the 4:1 resonance, i.e. $\Omega_{\text{b}} = \Omega + \kappa/4$, (Hunt and Bovy, 2018), which would imply a slower pattern speed. Alternatively, Hercules stream could be created (or interfered with) by transient spiral structure (Section 2.3.2), limiting our ability to measure the bar pattern speed from local data (e.g. Hunt et al., 2018, 2019).

More recent studies converge to a slower bar pattern speed. The kinematics of the gas in the bar region favors a slower pattern speed of about $\Omega_{\text{b}} = 40 \text{ km s}^{-1} \text{ kpc}^{-1}$ (Sormani et al., 2015). Also, thanks to NIR photometric and spectroscopic surveys, the kinematics of the stars in the bar are now directly measured. Comparison with kinematic models also suggests a lower pattern speed of around $33 - 40 \text{ km s}^{-1} \text{ kpc}^{-1}$ (e.g., Bovy et al., 2019; Sanders et al., 2019; Clarke and Gerhard, 2022). This slow pattern speed corresponds to the case of explaining the Hercules stream with co-rotation resonance of the bar.

Furthermore, Chiba et al. (2021) suggest that the kinematics of the Galactic disk stars can be used to measure the slowing-down of the pattern speed of the bar. Slowing down of the pattern speed of the bar is often seen in N-body simulations and it is a natural consequence of

the dynamical friction transferring angular momentum from the bar to the dark matter halo. They also suggest that the current pattern speed is around $35 \text{ km s}^{-1} \text{ kpc}^{-1}$, but that it was faster in the past.

Age of the bar

Bovy et al. (2019) measure the age and stellar abundance of the stars in the Galactic bar from the APOGEE data. They find that the stars in the bar are dominated by the old high- $[\alpha/\text{Fe}]$ stars like the thick disk. Hence, Bovy et al. (2019) suggest that the bar in the Milky Way formed at the same epoch as the formation of the thick disk. However, the age of the stars in the bar does not equate to the age of the bar, because stars older and younger than the formation age of the bar can be captured by the bar.

Bar formation is well known to induce gas inflow to the central sub-kpc of the galaxy, and create the nuclear gas disk. The stars formed in the nuclear gas disk build the nuclear stellar disk. Using a hydrodynamical galaxy evolution simulation including gas dynamics and star formation, Baba and Kawata (2020) demonstrate that the oldest age of the nuclear disk stars becomes consistent with the age of the bar, because they start forming after the bar forms.

Sanders et al. (2024) identify the Mira variable stars in the nuclear stellar disk of the Milky Way using the VVV data. Using the age-period relation of Miras calibrated in Zhang and Sanders (2023), they find that the Miras younger than about 8 Gyr show colder kinematics, i.e. their velocity dispersion is smaller. They conclude that the nuclear stellar disk started forming about 8 Gyr ago, and that it is also the time when the bar formed. This is a relatively less ambiguous measurement of the age of the bar, and it indicates the bar formed at an early epoch of the formation of the disk.

2.3.2 Spiral arms

Figure 1 shows the currently-believed spiral arm structure of the Milky Way. Note that this image is created by the extrapolations of the structures of the spiral arms inferred from a relatively small number (~ 200) of high-mass star-forming regions, whose distances are accurately measured by the radio Very Long Baseline Interferometer (VLBI) (Reid et al., 2019). The nearby stellar over-density structures of the spiral arms are also seen in the young OB stars in the Gaia data (e.g., Poggio et al., 2021), red clump stars (Lin et al., 2022), Cepheid variable, and HII regions (e.g., see Hou, 2021, for a review). Also, the spiral arms are identified with the systematic kinematical features (Eilers et al., 2020). However, the location or pitch angle of these arms are not always consistent with each other. Hence, the number of arms and the location of the arms are still under debate, and it remains challenging to identify spiral arm structure in the Milky Way disk.

The nature and the origin of the spiral arms remain controversial (e.g., see Dobbs and Baba, 2014, for a review). For a long time, the spiral arms have been believed to be a density-wave, where the stellar density-wave features are in a rigid-body rotation, despite the differential rotation of the stars (Lin and Shu, 1964). Kalnajs (1973) suggested a similar scenario called kinetic density-wave theory, which uses the closed ellipse orbit in the rotating frame with $\Omega_p = \Omega - \kappa/2$, which is called the Inner Lindblad resonance (ILR). The theory states that the angle of the major-axis of these closed elliptical orbits twists as a function of radius such that orbits align to make $m = 2$ spiral arm features. The speed of $\Omega_p = \Omega - \kappa/2$ is almost constant irrespective of radius for a normal galaxy's rotation curve, which helps maintain an almost stable feature for a long time. These kinetic density-wave spirals with the pattern speed of $\Omega_p = \Omega - \kappa/2$ are also created from the tidal interaction with another galaxy (e.g., Antoja et al., 2022) and also where the self-gravity of stars is not important, such as the outer disk (e.g., Hu and Sijacki, 2016).

On the other hand, in N-body simulations of an isolated Milky Way-sized disk galaxy, spiral arm features rotate at the same speed as the stars (the pattern speed being a decreasing function of radius for flat rotation curves), and hence are sometimes referred to as "co-rotating". This leads to individual spiral arms winding up and disappearing within a dynamical time (an epicycle period). However, spiral arm features are always present because although individual spiral arms disappear, new spiral arms form in other places of the disk, and are therefore called transient and recurrent structures (Sellwood, 2011). This scenario is sometimes called dynamic spiral arm scenario (Dobbs and Baba, 2014).

In the Milky Way disk, there is mixed observational support for both scenarios. The density-wave scenario predicts that star-forming gas, young stars, and the loci of spiral arms should be spatially offset, owing to the relative velocity difference between spiral arms and gas and stars. For example, from the compilation of various observational studies, Vallée (2021) claims that there are offsets between different spiral tracers, e.g. molecular gas and different ages of stars, and suggests a spiral arm pattern speed of $\Omega_{\text{sp}} = 12 - 17 \text{ km s}^{-1} \text{ kpc}^{-1}$. In addition, several studies suggest that the moving groups found in the distribution of the radial and rotation velocities of stars in the solar neighborhood, as well as the ridge-like features in the rotation velocity distribution as a function of the radius (Section 2.4), can be explained by the kinetic density-wave scenario. For example, using test particle simulations (i.e. no self-gravity) with the spiral arm potentials with a rigid-body rotation, Barros et al. (2020) demonstrate that the phase space features observed in the Gaia data are reproduced with the $m = 4$ spiral arms with the pitch angle of 14° and the pattern speed of $\Omega_{\text{sp}} = 28.5 \text{ km s}^{-1} \text{ kpc}^{-1}$.

On the other hand, Castro-Ginard et al. (2021) find that open clusters with different ages seem to show no offset, and conclude that the pattern speeds of the spiral arms consistent with the rotation speed of stars in the radial range between 5 and 12 kpc. This is more consistent with the dynamic spiral arm scenario. The observed vertical (Asano et al., 2024) and in-plane (Funakoshi et al., 2024) kinematics in the spiral arm traced by high-mass star-forming regions is consistent with what is seen in N-body simulations with dynamic arms. Comparing kinematics of Cepheid variables around the spiral arms with N-body simulations, Funakoshi et al. (2024) suggest that the Local and Outer arms are growing, while the Perseus arm is disrupting, which supports the transient, recurrent nature of dynamic spiral arms.

The tension of these scenarios remains even with the exquisite observational data now available for the Milky Way disk. This is partly because of our location within the Galactic disk, and we cannot see a clear picture of the structure of the disk from the outside. To resolve the tension of these scenarios, we need to more clearly identify the location of the spiral arms in the Milky Way disk, especially with relatively

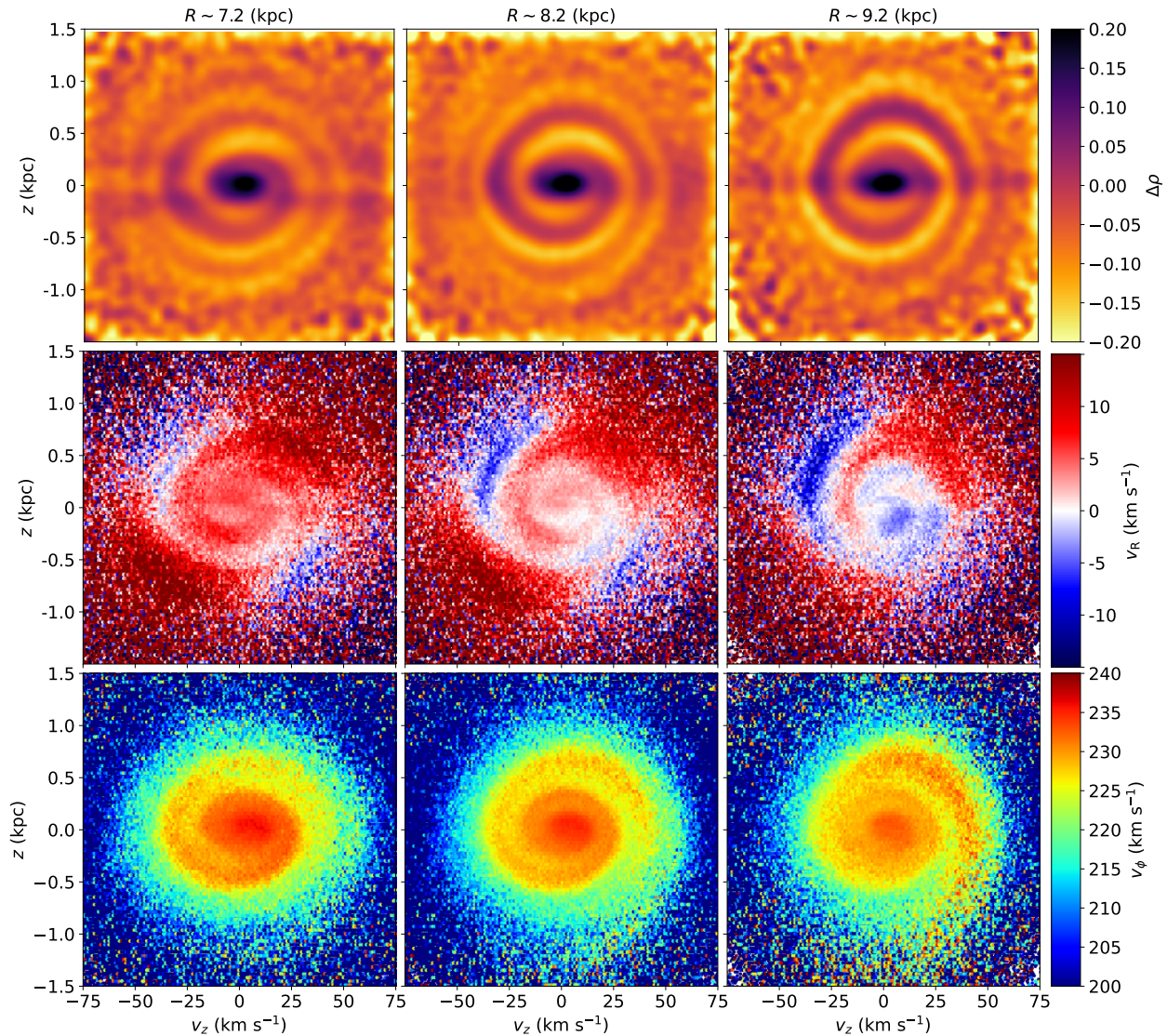


Fig. 3 ‘Phase spirals shown in relative density (upper row), as a function of radial velocity, V_R (middle row), and azimuthal velocity, V_ϕ (lower row) for 1 kpc volumes of Gaia DR3 data centered around $R = 7.2$ kpc (left column), $R = 8.2$ kpc (i.e. the Solar neighborhood; middle column) and $R = 9.2$ kpc (right column); see e.g. Antoja et al. (2018, 2023).

older thin disk stars, which trace the gravitational potential of the arms. Also, the spiral arms in the Milky Way could be flocculent, as suggested by several studies (e.g., Colombo et al., 2022). More observational data and comparison with simulation models are required to understand the nature and structure of the spiral arms of our Galaxy.

2.3.3 Impacts of the bar and spiral arms: radial migration

Non-axisymmetric structures like the bar and spiral arms give rise to “co-rotation resonances”: special radii where the bar/spiral arms rotate at the same speed as the stars. Sellwood and Binney (2002) show that the co-rotation resonance of the spiral arms and bars can induce significant radial migration of stars. This phenomenon occurs when stars lose and/or gain angular momentum as a result of gravitational torques imparted by non-axisymmetric structures, which causes stars to change their guiding center radii: the radius where stars on circular orbits of a given angular momentum would occupy. The terminology of “radial migration” or “radial mixing” is used for the change of the angular momentum of stars with or without orbital heating (an increase in orbital eccentricity). Schönrich and Binney (2009) dubbed the change in the angular momentum as “churning”, and the increase in the amplitude of the radial epicycle motion, or orbital heating, as “blurring”. Radial migration due to a co-rotation resonance as suggested by Sellwood and Binney (2002) corresponds to churning without blurring.

The process of radial migration complicates Galactic archaeology studies because the current angular momentum of some stars will likely be quite different from their angular momentum at birth. Schönrich and Binney (2009) include churning and blurring in a multi-zone

Galactic chemical evolution model and demonstrate that the radial mixing of stars helps to explain the scatter of the age metallicity relation observed for the solar neighborhood stars (Section 3), and also the bimodal distribution of the high- $[\alpha/\text{Fe}]$ and low- $[\alpha/\text{Fe}]$, chemically-defined thick and thin disk populations (Figure 2).

Using numerical simulations of a Milky Way-sized galaxy, Grand et al. (2012) show that because the dynamic spiral arm is co-rotating at all radii, radial migration occurs at every radius. In this case, the stars migrating outward stay on the trailing side of the spiral arm, gaining torque from the arm and staying close to the apo-center phase of their orbit. On the other hand, stars migrating inward stay on the leading side of the spiral arm, losing angular momentum and staying close to peri-center phase. It means that the dynamic spiral arms induce the systematic radial migration around the spiral arms at every radius. Finding such radial migration in action could resolve the tension on the nature of spiral arms (Section 2.3.2).

Frankel et al. (2020) fit the APOGEE data with an analytical disk galaxy model with parameters describing the inside-out formation of the disk as well as churning and blurring. They assume that stars formed on circular orbits and with a metallicity inherited from their natal star-forming gas; the radial metallicity profile of the gas disk is described with a constant metallicity gradient and an intercept that changes with time. Under these assumptions, each star has a unique metallicity that depends on their formation radius and time. On top of this, their model includes churning and blurring and sets the efficiencies of these processes as fitting parameters. Their best-fit model indicates that churning is more important than blurring in the Milky Way disk, which suggests that radial migration due to the co-rotation resonance is more important than heating. Interestingly, Okalidis et al. (2022) show that cosmological numerical simulations of Milky Way-mass spiral galaxies predict a similar amount of churning to what is reported by Frankel et al. (2020).

Using the same logic of a star-forming gas disk with a negative metallicity gradient and no scatter, the birth radii of stars can be inferred from their age and metallicity (Minchev et al., 2018). Because the Sun’s metallicity is higher than the stars around us, it is likely that the Sun radially migrated from the inner disk at around $R = 5 - 7$ kpc (Wielen et al., 1996). By analyzing the orbits of the stars migrating from the inner disk to the solar radius in an N-body simulation, Tsujimoto and Baba (2020) discuss that if the Sun migrated significantly, during the migration the Sun needed to stay close to the spiral arm for a long time, which may have affected the Earth’s environment, and therefore may be associated to historical events like snowball Earth, when all water on the Earth surface was frozen. Hence, the radial migration process of the Sun could be constrained by the geological history of the Earth, and/or the history of the Earth could be closely related to the past journey of the Sun in the Milky Way disk.

2.4 Galactoseismology: Phase Spirals/Ridges/Corrugations

2.4.1 Phase spirals and ridges

One of the most striking discoveries of the Gaia data which impacted our view of the Milky Way disk is the fine sub-structure in the phase space distribution of the Milky Way disk stars (e.g., Antoja et al., 2018; Kawata et al., 2018). Antoja et al. (2018) find that the distribution of the vertical position of stars relative to the mid-plane of the disk, z , and the vertical velocity of stars, V_z , in Gaia DR2 shows a $m = 1$ spiral pattern. Figure 3 shows this spiral pattern in Gaia DR3 data at three different galactic radii, slightly inside the Solar radius (left column), in the Solar neighborhood (center column) and slightly outside the solar radius (right column). The spiral in number density is clearly visible in relative density, $\Delta\rho$, when subtracting a smooth background distribution as shown in the upper row. The feature is also prominent when highlighted with the rotation velocity (lower row), V_ϕ , or radial velocity, V_R (middle row), i.e. the vertical and in-plane kinematics are correlated.

This feature is now called “phase spirals”. With data from Gaia DR3, the phase spiral has been mapped across a large region of the Galactic disk in both physical space (e.g. Antoja et al., 2023), and as a function of orbital parameters (e.g. Hunt et al., 2022). Distinct $m = 2$ arm phase spirals have been discovered in the inner disk (Hunt et al., 2022), and equivalent phase spirals are seen in the radial direction $\Delta R - V_R$ (Hunt et al., 2024). All these phase spirals are the signature of phase mixing following some perturbation to the disk, the origin of which is discussed in Section 2.4.3 (and see Hunt and Vasiliev, 2024, for a thorough review).

Kawata et al. (2018) and Antoja et al. (2018) show that there are many ridge-like features in the stellar distribution of the rotation velocity, V_ϕ , as a function of radius, R . They are now known to be the radial extension of the moving groups first identified by Olin Eggen in the $V_\phi - V_R$ phase space plane for the solar neighborhood stars (see Eggen, 1996, and references therein). Fragkoudi et al. (2019) show that the ridge-like features in the $R - V_\phi$ plane are correlated with V_R as well. Figure 4 shows the classic $V_R - V_\phi$ plane with a rough illustration of the moving groups (left). The middle panel shows the $R - V_\phi$ plane in number density, where it can be seen that these diagonal ridge-like features stretch over several kpc in the disc. The right panel shows the $R - V_\phi$ plane as a function of V_R , with the rough location of the moving groups marked, with colors that match the groups in the left panel.

2.4.2 Corrugations and warp

Using Gaia DR1 Schönrich and Dehnen (2018) revealed a wave-like feature in V_z as a function of the angular momentum of the stars. Friske and Schönrich (2019) build on this with Gaia DR2 data, finding the wave-like feature is also present in the radial velocities, v_R as a function of angular momentum. The vertical, V_z , and in-plane radial, V_R , velocities are likely related to each other and due to a common origin and/or one induces the other, as discussed below.

Cepheid variables are young (a few 100 Myr old) variable stars, and are known to be a standard candle to provide precise distances, because their absolute magnitude is correlated to the period of their flux variations. Hence, the distances to Cepheids can be measured more precisely than the parallax measurement of Gaia especially at a larger distance ($d \gtrsim 5$ kpc). Skowron et al. (2019) map the spatial distribution of about 2000 Cepheids in the Milky Way disk and reveal clearly the structure of the warp in the Galactic outer disk up to about $R = 20$ kpc. We define $\phi = 0$ as the Sun–Galactic center line of the Galactocentric azimuthal angle, ϕ , and ϕ to be positive in the direction

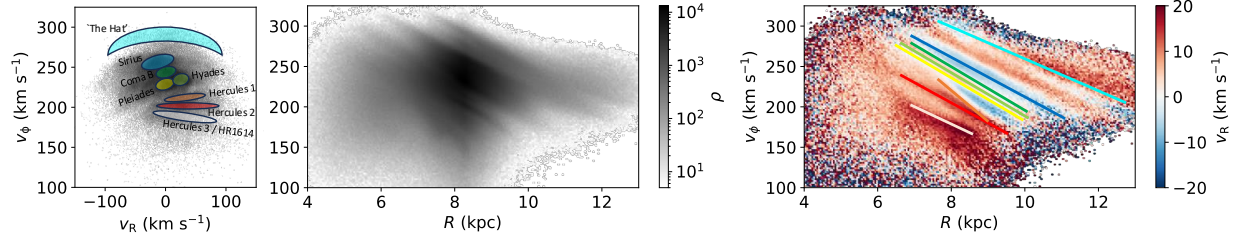


Fig. 4 **Left:** $V_R - V_\phi$ plane with the classical moving groups marked. **Center:** $R - V_\phi$ plane in number density. **Right:** $R - V_\phi$ plane as a function of radial velocity, V_R , with the rough location of the moving groups marked, matching the colors from the left panel (see e.g. Hunt et al., 2019).

of Galactic rotation, as shown in Figure 1. At $R \gtrsim 10$ kpc, the disk bends downward behind the direction of rotation of the Sun, i.e. at $\phi < 0$, while at positive ϕ it goes upward. The observed amplitude is about $\Delta|z| \sim 1$ kpc at $R \sim 15$ kpc. Hence, the line of nodes of the warp is close to the Sun–Galactic center line, but it is slightly on the positive ϕ side. Chen et al. (2019) suggest that the line of nodes of the warp is twisted, i.e. it has a different angle at different radii, which is a sign of the precession of the warp. Using Gaia DR2 data and analyzing the position and kinematics of about 12 million giant stars, Poggio et al. (2020) measure the precession of the warp to be about $11 \text{ km s}^{-1} \text{ kpc}^{-1}$, where the positive value means the warp is precessing in the same direction as the rotation of the disk. However, the exact shape of the line of nodes and the speed of the precession are hotly debated, and our view of the outer edge of the Galactic disk requires further exploration.

Furthermore, Poggio et al. (2024) subtract the general trend of the disk bending due to the warp and analyse the remaining structures present in the Gaia data. They find the vertical corrugation in the young (<a few 100 Myr) disk stars is propagating outward. They suggest that this vertical corrugation reaches up to $|z| \sim 150 - 200$ pc and has a radial length of about 3 kpc. The corrugation is seen up to $R \sim 20$ kpc when traced by the Cepheids.

This vertical corrugation is also found in the star-forming gas filaments. Alves et al. (2020) have discovered a filamentary gas structure, which shows a vertical wave-like feature with a vertical amplitude of about 160 pc and wavelength of 2 kpc, around the Sun, called the Radcliffe wave. This wave spans about 3 kpc along the inside of the Local arm. The wavelength in the radial direction is about 1 kpc, which is significantly shorter than the corrugation seen in the young stars in Poggio et al. (2020). It is not yet clear if or not they are related to each other.

The older stars in the disk seem to show even more spectacular vertical wave-like features. In the anti-center direction, several over-density structures are observed and spread to high Galactic latitudes up to about $|b| = 30^\circ$. Bergemann et al. (2018) take high-resolution spectra for the red giant branch stars associated with two of these structures, called the Triangulum–Andromeda (TriAnd) and A13 overdensities, and obtain their chemical compositions. From the similarity of their abundances to the Galactic thin disk, they conclude that both TriAnd and A13 are part of the outer thin disk. The A13 structure is at around $R = 16$ kpc, and TriAnd is around $R = 28$ kpc. Also, A13 is above the mid-plane of the inner disk by about $z = 5$ kpc, while TriAnd is below by 5 kpc. This is a much bigger amplitude than the warp seen in the younger stars. In addition, TriAnd is located at $\phi \sim 30^\circ$, where the warp bends upward, and A13 is around $\phi = 0^\circ$, which is close to the line of nodes of the warp. Hence, the older stars seem not to follow the warp, but have their own vertical corrugation mode in the outer disk.

2.4.3 The sources of the perturbation

A number of theoretical studies and numerical simulation studies have been published since Gaia uncovered the velocity substructures in the Galactic disk. Antoja et al. (2018) suggest that the phase spiral they find in the Gaia data arises from phase mixing from an out-of-equilibrium condition caused by some perturbation. From the wraps of the phase spiral, they suggest that the impact was 300 – 900 Myr ago, which is a similar time to the expected last passage of the Sagittarius dwarf galaxy. It is also demonstrated that a Sagittarius dwarf-like perturber can produce phase spiral-like features (e.g. Laporte et al., 2019). However, the required mass of the perturber to have sufficient impact on the disk is higher than the currently estimated mass of the Sagittarius dwarf. Although several simulations are able to qualitatively reproduce such phase spirals, none have yet reproduced the specific configuration (amplitude, pitch angle, and phase as a function of Galactic position) seen in Gaia from a Sagittarius dwarf-like simulation (e.g. Bennett et al., 2022, and references therein).

There are alternative mechanisms that can create phase spirals. As explained above, single-armed phase spirals can be created by the displacement of the phase space distribution of the stars in $z - V_z$ phase space. Hence, any vertical corrugation can trigger such $m = 1$ phase spirals. Using N-body simulations, Khoperskov et al. (2019) demonstrate that the bar buckling, which may occur when the BPX-bulge is created in the Milky Way disk, can trigger such a vertical wave and generate the phase spirals seen in the disk. However, BPX-bulges can also form through resonant growth without undergoing a buckling instability, and the nature of the Milky Way’s BPX-bulge is still debated (see e.g. Baba et al., 2022, for an example of the BPX-bulge formation without buckling).

Alternatively, the phase spirals can be created by interaction with dark matter. Tremaine et al. (2023) show that stochastic bombardment of the disk by dark matter subhalos can cause long-lived phase spirals. Grand et al. (2023) show that earlier interactions of the Milky Way with the Sagittarius dwarf galaxy when it was much heavier can induce a significant wake in the Milky Way’s dark matter halo which lasts

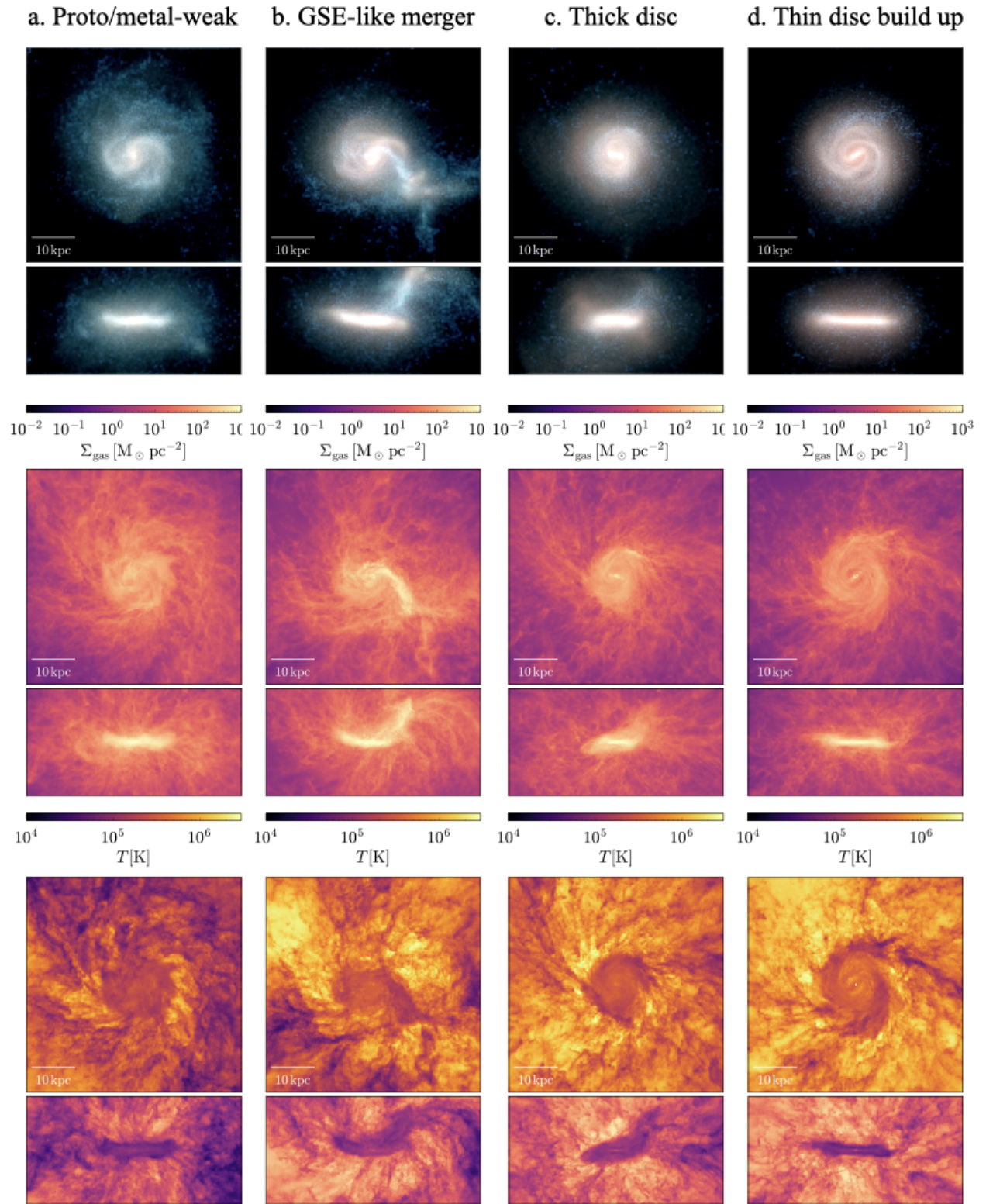


Fig. 5 Simulation snapshots depicting important stages of disk formation. The top-, middle-, and bottom-rows show the the face-on and edge-on view of stellar light (blue and red indicate young and old stars, respectively), gas density, and gas temperature at each stage, respectively. The highlighted stages are: a) the metal-weak proto-disk at early epochs; b) the GSE merger event; c) the thick disc formation; and d) the build-up of the thin disk.

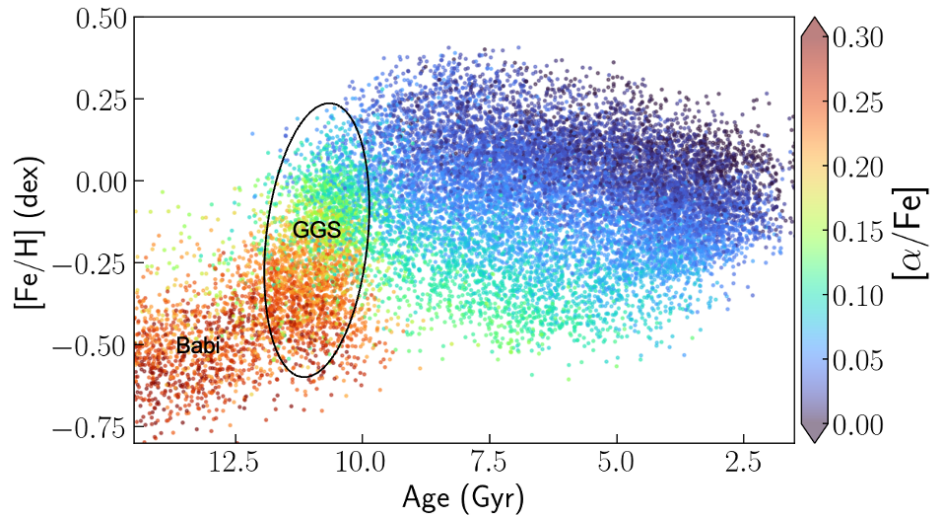


Fig. 6 The age-metallicity relationship of APOGEE DR17 giants (the same sample as Figure 2). The colour of the dots indicates $[\alpha/\text{Fe}]$. We highlight the older population Babi and the GGS (see text).

for several Gyr. This wake can then continue to perturb the disk long after the initial interaction, potentially creating and maintaining the phase spirals until the present day even after Sagittarius has lost most of its mass.

Regardless of the origin of the perturbation, the perturbation(s) likely caused both the corrugations and the phase spirals, and possibly the warp. As mentioned above, the phase spirals are well correlated with the in-plane motion, such as the radial and azimuthal motion of the stars. The vertical corrugation and spiral arms in the disk could also be related to each other. In fact, a tidal interaction, such as the impact of the Sagittarius dwarf, can trigger both vertical corrugations and in-plane spiral arm features, as demonstrated by Bland-Hawthorn and Tepper-García (2021). In fact, spiral arms can also trigger vertical breathing motion, i.e. expansion and compression motion (Debatista, 2014; Asano et al., 2024). Such breathing motion can induce two armed phase spirals, such as those found by Hunt et al. (2022). It is likely that the vertical motion and in-plane motions are coupled to each other, and modelling both together is likely key to breaking the degeneracies between the various models.

3 The formation of the Milky Way disk: Proto-disk, Thick disk, and Thin disk

The recent advance of computing power and significant improvements in modeling the physics of galaxy formation have enabled computer simulations to follow the formation and evolution process of Milky Way-like galaxies from very high redshifts (e.g. $z \sim 100$) until the present-day. These simulations demonstrate that, under the current standard Λ -dominated cold dark matter (Λ CDM) cosmogony, Milky Way-like disk galaxies inevitably experience chaotic mergers at early epochs of formation. To build a Milky Way-like disk galaxy with a prominent thin disk, this period should be followed by a longer term ($\sim 8 - 10$ Gyr) quiet phase characterized by the gradual build-up of the thin disk in the absence of major mergers (although minor mergers and galactic interactions can occur; Brook et al., 2004; Grand et al., 2018). This thin disk is where the majority of the Milky Way's stars now reside. Although simulations also show that a thinner disk can form at early epochs, the prevalence of merger events ensures that such a disk would sustain repeated dynamical impacts that scatter stars onto orbits that would now be observed as part of the thick disk and stellar halo.

In the Gaia data, there is evidence that the early epoch of merger activity concluded around 8 – 10 Gyr ago with a significant merger known as Gaia-Sausage-Enceladus (hereafter GSE, Belokurov et al., 2018; Helmi et al., 2018), the stellar debris of which makes up about half of the stellar halo. Interestingly, signs of satellite accretion in the stellar halo have been claimed with the ESA's Hipparcos data. Brook et al. (2003) note that the combination of the Hipparcos data and the line-of-sight velocity and metallicity information from spectroscopic surveys shows a group of stars with low metallicity on high-eccentricity orbits, as seen also in the historical Eggen et al. (1962) work. However, rather than regarding this group of stars as evidence of the rapid collapse of the Milky Way halo as considered in Eggen et al. (1962), Brook et al. (2003) used comparisons with their numerical simulations to demonstrate that the phase space distribution of this group of stars is more naturally explained by the remnants of a dwarf galaxy accreted into the Milky Way in the past. Now, it is clear that the phase space distribution of the group of stars they found is consistent with that of the GSE stars found in the Gaia data. Aside from clear differences in their orbital characteristics, many studies (e.g., Haywood et al., 2018; Helmi et al., 2018) show also that the chemical abundances of GSE stars are different from those that are likely "in-situ" stars, i.e. stars formed within the main progenitor of the Milky Way. These findings agree with earlier results found prior to Gaia by Nissen and Schuster (2010).

The Gaia data show also that the GSE merger has a significant impact on the "in-situ" stars that were already formed at the time of the merger: these stars were "splashed" out of the disk and into halo, and are currently observed as relatively metal-rich halo stars compared to

the GSE remnants. This component of the stellar halo was identified by Di Matteo et al. (2019) and Gallart et al. (2019), and was dubbed the "Splash" by Belokurov et al. (2020). This means that the Galactic disk was already building up well before the GSE merger. This proto-Galactic disk is claimed to be identified by Belokurov and Kravtsov (2022): they found that the median rotation velocity of metal-poor stars increases sharply, or is "spun-up", in the metallicity range $[\text{Fe}/\text{H}] \sim -1.5$ to $[\text{Fe}/\text{H}] \sim -0.9$. They call this component "Aurora". Similar trends are found in results summarised by various metaphors such as the "boiling hot" phase and the "poor old heart" by Conroy et al. (2022) and Rix et al. (2022), respectively. Interestingly, these new studies are consistent with what is found in the Hipparcos data of the solar neighborhood stars in Chiba and Beers (2000), who established the clear increase of the mean rotation velocity of stars with metallicity at $[\text{Fe}/\text{H}] > -1.7$. These studies show also that this metal-poor spin-up component is old and centrally concentrated. Hence, this is likely to be the starting phase of the Milky Way disk, which unsurprisingly began from a smaller, metal-poor disk.

Proto-disk galaxies such as these likely experienced many mergers. Because they are still too small to establish the hot gas halo, their mergers are likely to be gas-rich mergers. Thanks to the dissipative nature of gas, gas-rich mergers lead to a disk-like galaxy (Robertson et al., 2006; Brook et al., 2007), though it may not be as thin as the disk galaxies of today. In addition, as suggested by Noguchi (1998) with his numerical simulations, thermal instability is quite efficient in gas-rich disks at early epochs, and this likely generates large star-forming clumps that continuously puff-up the disk through dynamical scattering. As mentioned above, the GSE merger splashed some proto-disk stars onto eccentric, halo-like orbits. However it is likely that some fraction of proto-disk stars remain in what is now regarded as the thick disk (Grand et al., 2020).

The GSE merger is now considered to be the last significant galaxy merger for the Milky Way. It follows that the Milky Way has had about 8 – 10 Gyr of evolution during which no major merger has occurred. In such a quiet period, the galaxy is thought to have built a thin disk via the smooth accretion of halo gas; gas with higher angular momentum falls onto the disk at later epochs (Brook et al., 2011) and, as such, builds the thin disk in an inside-out fashion (Brook et al., 2004). The Milky Way's current mass is just above the mass threshold required to develop the hot halo gas, i.e. "hot-mode" (Kereš et al., 2005), which cuts-off the direct cold filamentary accretion onto the disk by shock-heating cold gas flows. However, the Milky Way has not always been this massive and must have been under this mass threshold at earlier epochs during which cold flows are not shock heated by the halo gas and instead accrete unimpeded directly onto the disk. Noguchi (2018) suggest that the transition from thick disk formation to thin disk formation is because of the transition from cold mode accretion to hot mode accretion as the Milky Way surpasses the mass threshold.

Using self-consistent cosmological (magneto-)hydrodynamical simulation of a Milky Way-sized galaxy, Grand et al. (2018) showed that it is possible for such a transition to happen for Milky Way-sized galaxies. Further, Grand et al. (2020) demonstrated that the GSE-like merger can trigger this transition by boosting the total mass of the Milky Way, thus aiding thin disk formation from subsequent smooth, hot-mode gas accretion. Figure 5 shows a sequence of snapshots depicting the stages of disk formation described above, taken from the Auriga-18 cosmological simulation. The top-, middle-, and bottom-rows show the the face-on and edge-on view of stellar light, gas density, and gas temperature at each stage, respectively. At the earliest epoch (column a), the relatively small proto-disk/metal-weak disk forms in the presence of minor mergers and cold-mode gas accretion. Column b) shows the gas-rich GSE merger event, which both scatters stars into the thick disk and "Splash" halo components and induces a starburst by compressing gas into a dense, compact form that contributes to a significant part of the thick disk (column c). Coincident with the finalization of these processes is the increase of halo gas temperature, which marks a transition to hot-mode accretion and the growth of the thin disk (column d). Like many other studies (e.g., Brook et al., 2004; Bird et al., 2013; Agertz et al., 2021), these simulations show that the gas disk becomes thinner with time, and thus the thin disk forms "upside-down" as well as inside-out. Interestingly, they show also that the gas and stars belonging to the thin disk evolve with a flared scale-height profile qualitatively similar to the Milky Way thin disk as described in Section 2.2.

The predicted impact of the GSE merger and subsequent thin disk formation are also qualitatively consistent with the precise chemical abundance measurements from the APOGEE survey and the kinematics from the Gaia data (see Deason and Belokurov, 2024, for a review). Advanced data analysis techniques now allow us to infer reliable stellar ages, which is crucial information for the archaeological study of the Milky Way's formation and evolution history. Ciucă et al. (2024) analyse the age-metallicity relation of APOGEE giant stars (Figure 6), and identify three phases of the Milky Way formation: the metal-poor proto-disk phase, which they called "Babi"; a rapid increase in metallicity in a short time, which they dubbed the "Great Galactic Starburst (GGS)"; followed by the metal-rich thin disk formation phase. Note that the Babi corresponds to the late stage of the spin-up phase (like Aurora) because Figure 6 focuses on the stars after the proto-disk is established at $[\text{Fe}/\text{H}] > -1$. The subsequent rapid increase of metallicity in the GGS phase supports the idea that the GSE merger was a gas-rich galaxy merger, which would trigger a starburst and in turn spur the rapid chemical enrichment of gas and successive generations of stars. The lowest metallicity component, i.e. the beginning of GGS, also shows high $[\alpha/\text{Fe}]$. This also indicates the rapid increase of SNe II that naturally follow from an increase in star formation rate as a result of the gas-rich merger.

From the age- $[\text{Fe}/\text{H}]$ - $[\alpha/\text{Fe}]$ relation of the APOGEE giants data, Ciucă et al. (2021) suggest that there is a transition phase, which they called "the Bridge", between the high- $[\alpha/\text{Fe}]$ thick disk and the low- $[\alpha/\text{Fe}]$ thin disk populations (Figure 7). Such transition population of stars are also noted in the earlier studies, such as Adibekyan et al. (2013). Ciucă et al. (2021) show that, in the Bridge, $[\alpha/\text{Fe}]$ decreases with age, and the width of the range of $[\text{Fe}/\text{H}]$ at fixed age increases also. Their interpretation is that, during the high- $[\alpha/\text{Fe}]$ thick disk formation phase before the Bridge, the prevalence of gas-rich mergers and cold-mode accretion drive a high degree of turbulence that leads to a well-mixed gas disk. After the GSE merger settled, which corresponds to the beginning of the Bridge, the thin disk grows in mass and size such that a radial metallicity gradient (with higher metallicity in the inner disk) develops, which leads to a wider range of metallicities for younger thin disk stars. As mentioned above, although the star-forming gas disk could have a clear metallicity gradient with no metallicity variation at a fixed radius, radial migration brings stars formed in both the inner and outer disk to the solar neighborhood. Hence, we can observe a wide variety of metallicity of both young and old thin disk stars (Schönrich and Binney, 2009). The transition from the thick disk phase, which, we consider, happened only in the inner disk, to the thin disk phase are summarized in the observed $[\text{Fe}/\text{H}]$ - $[\alpha/\text{Fe}]$ relation,

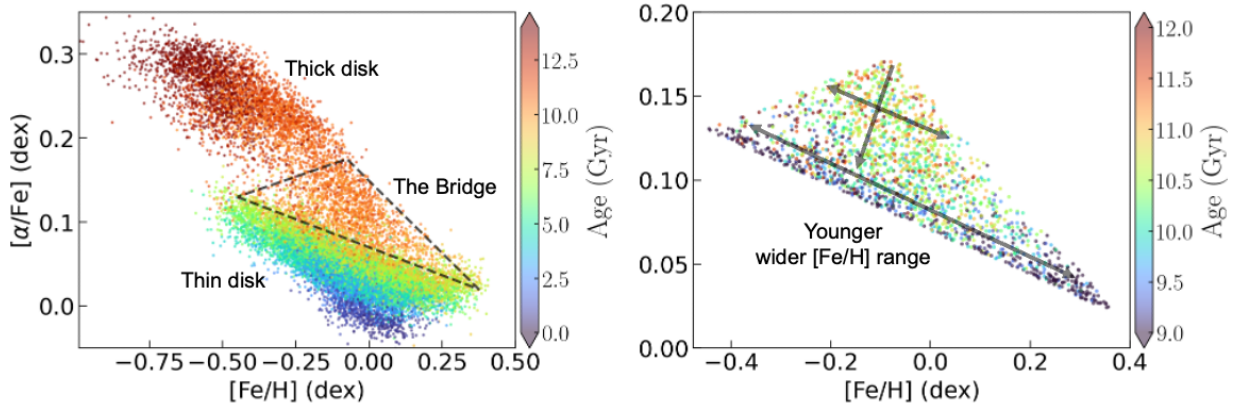


Fig. 7 The distribution of $[\alpha/\text{Fe}]$ and $[\text{Fe}/\text{H}]$ colored by age for stars in Figure 2. The dashed triangle region in the left-hand panel is referred to as the Bridge, and is a transition region between the thick (old high- $[\alpha/\text{Fe}]$ population) and thin (young low- $[\alpha/\text{Fe}]$ population) disks. An age gradient is apparent, as indicated by the near vertical downward arrow, in a close-up of the Bridge region, shown in the right-hand panel, and the range of $[\text{Fe}/\text{H}]$ becomes wider, as indicated by the double arrows for the younger stars in the Bridge region.

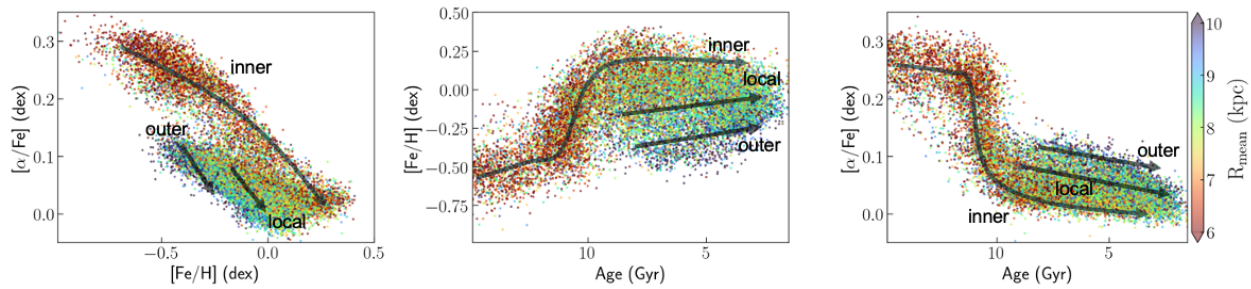


Fig. 8 The distribution in $[\alpha/\text{Fe}]$ versus $[\text{Fe}/\text{H}]$ (left-hand panel), $[\text{Fe}/\text{H}]$ versus age (middle panel), and $[\alpha/\text{Fe}]$ versus age (right-hand panel) coloured by mean orbital radius, R_m . The ‘inner’, ‘local’, and ‘outer’ arrows indicate the schematic chemical evolution paths at the inner ($R_m \sim 6$ kpc), local, i.e. solar radius ($R_m \sim 8$ kpc), and outer discs ($R_m \sim 10$ kpc), respectively. The metal-poor, outer disk stars follow a different chemical evolution pathway than the inner disc. These evolutionary paths are shown to describe qualitative trends of the chemical evolution at the different radii of the Galactic disk, and are not meant to indicate the chemical evolution paths quantitatively. Adapted from Ciucă et al. (2021).

age- $[\text{Fe}/\text{H}]$ relation, and age- $[\alpha/\text{Fe}]$ relation in Figure 8. The schematic chemical evolution pathways are indicated in the figure. Note that the absolute value of the age used in Figures 6-8 is less meaningful, but the relative difference of the ages is precise and meaningful. Although the stars should not be older than the age of the Universe, the prior of the age of the Universe is not used, because the prior of the old age limit forces the inferred age of the old stars to be similar. Hence, the inferred ages are allowed to exceed the age of the Universe. This helps to make the relative age difference between the old stars more clear.

Similar scenario to arrows in Figure 8 is suggested by Haywood et al. (2019), although they consider that the outer thin disk formed earlier than the inner thin disk population. Note also that the arrows in Figure 8 are only schematic trends merely reflecting the authors’ current view. More data with the accurate age measurements are crucial to fully understand how the transition from the thick disk to thin disk formation happened, how the GSE impacted on it, and if the bar formation, which is likely around similar time (Section 2.3.1), is also related to this transition (e.g., Mewer et al., 2024).

4 Summary and Future Prospects

The Gaia mission and both photometric and spectroscopic surveys of the Galactic stars have revolutionised our view of the Milky Way disk. The Milky Way disk is no longer considered to be a quiet stable disk galaxy, but is rather an out-of-equilibrium structure reeling from perturbation(s) caused by accreting satellites and/or dark matter halo. This leads to many challenges for us to accurately measure the mass and size of the Milky Way disk, and use the Galactic disk stars to infer the density of the dark matter. However, a challenge is always an opportunity. The data from Gaia and complementary surveys keep improving and our understanding of the phase space sub-structures is advancing. More precise measurements of these motions and comparisons with dynamical models and numerical simulation must allow us to use such seismic information of the Milky Way disk to infer both the nature of the waves, including the bar and spiral arms, and the composition of the Galaxy, including the density profiles of the stellar disk and dark matter.

In addition to the upcoming Gaia DR4 with five years of the Gaia mission data and the final data release of more than ten years of data, further advances of observational data are anticipated. The Prime Focus Infrared Microlensing Experiment (PRIME)⁵, a wide field 1.8 m telescope with a NIR camera at the South African Astronomical Observatory, started the inner Milky Way region survey. The Vera C. Rubin Observatory's the Legacy Survey of Space and Time (LSST)⁶ is planned to begin in 2025, and will provide time series photometric data in the large region of the Southern hemisphere sky, including the Galactic bulge/bar region. Ground-based spectroscopic surveys with the next generation multi-object spectrograph in the Southern hemisphere, such as optical 4-meter Multi-Object Spectrograph Telescope (4MOST)⁷ on the Visible and Infrared Survey Telescope for Astronomy (VISTA) telescope and NIR Multi-Object Optical and Near-infrared Spectrograph (MOONS)⁸ on VLT will further add value to these data and will help us understand the kinematics and stellar abundance distributions of the inner Milky Way disk. In the Northern hemisphere, WHT Enhanced Area Velocity Explorer (WEAVE)⁹ on the William Herschel Telescope (WHT) and Prime Focus Spectrograph (PFS)¹⁰ on Subaru will start science surveys soon, and will provide valuable data for the outer disk and halo stars. These data will help understand the holistic view of the Milky Way's disk formation and perturbation histories and how they are related to the subtle features in the halo stars.

As described in this chapter, stars are crucial tracers and fossil records to tell us the formation history of the Galaxy. Hence, understanding stellar physics is critical for Galactic astronomy and a wide range of astronomy research. Asteroseismology is now a critical tool for understanding stellar physics. The proposed space mission, High-precision Asteroseismology in DeNse stellar fields (HAYDN, Miglio et al., 2021b)¹¹, plans to measure the precise time-series photometry of stars in star clusters with homogeneous age and abundances. This will finally allow us to calibrate stellar physics models and will help us to accurately measure the ages of stars.

Because Gaia is an optical survey, astrometry of stars found in line-of-sights toward the Galactic center is limited to within a few kpc from the Sun. The Japan Astrometry Satellite Mission for Infrared Exploration (JASMINE, Kawata et al., 2024)¹² NIR space astrometry mission by ISAS/JAXA will provide precise astrometry for the stars between the Galactic center and the Sun, although their survey region is focused on only the Galactic center region ($< \sim 1.5^\circ$). Ultimately, the ESA's future planned L-mission, GaiaNIR¹³ (Hobbs et al., 2021), will provide NIR all-sky astrometry of similar precision and depth to Gaia, but in NIR. The GaiaNIR mission is expected to be able to measure astrometry for about eight billion stars, including the stars in the Galactic disk mid-plane and the stars around the super-massive black hole in the center of the Milky Way. In addition, the next-generation of radio telescopes, such as Square Kilometer Array (SKA)¹⁴ and Next Generation Very Large Array (ngVLA)¹⁵, will also provide information on the gas, star formation, and magnetic fields. These multi-wave future surveys of the Milky Way will help uncover the formation process of the Milky Way disk - where our Sun was born and where we live.

Acknowledgments

This work is a part of MWGaiaDN, a Horizon Europe Marie Skłodowska-Curie Actions Doctoral Network funded under grant agreement no. 101072454 and also funded by UK Research and Innovation (EP/X031756/1). This work was also partly supported by the UK's Science & Technology Facilities Council (STFC grant ST/S000216/1, ST/W001136/1). RJG is supported by an STFC Ernest Rutherford Fellowship (ST/W003643/1).

This work has made use of data from the European Space Agency (ESA) mission *Gaia* (<https://www.cosmos.esa.int/gaia>), processed by the *Gaia* Data Processing and Analysis Consortium (DPAC, <https://www.cosmos.esa.int/web/gaia/dpac/consortium>). Funding for the DPAC has been provided by national institutions, in particular the institutions participating in the *Gaia* Multilateral Agreement.

Funding for the Sloan Digital Sky Survey IV has been provided by the Alfred P. Sloan Foundation, the U.S. Department of Energy Office of Science, and the Participating Institutions. SDSS acknowledges support and resources from the Center for High-Performance Computing at the University of Utah. The SDSS web site is www.sdss4.org. SDSS is managed by the Astrophysical Research Consortium for the Participating Institutions of the SDSS Collaboration including the Brazilian Participation Group, the Carnegie Institution for Science, Carnegie Mellon University, Center for Astrophysics — Harvard & Smithsonian (CfA), the Chilean Participation Group, the French Participation Group, Instituto de Astrofísica de Canarias, The Johns Hopkins University, Kavli Institute for the Physics and Mathematics of the Universe (IPMU) / University of Tokyo, the Korean Participation Group, Lawrence Berkeley National Laboratory, Leibniz Institut für Astrophysik Potsdam (AIP), Max-Planck-Institut für Astronomie (MPIA Heidelberg), Max-Planck-Institut für Astrophysik (MPA Garching), Max-Planck-Institut für Extraterrestrische Physik (MPE), National Astronomical Observatories of China, New Mexico State University, New York University, University of Notre Dame, Observatório

⁵<http://www-ir.ess.sci.osaka-u.ac.jp/prime/index.html>

⁶<https://rubinobservatory.org/>

⁷<https://www.4most.eu/cms/home/>

⁸<https://vl moons.org/>

⁹<https://weave-project.atlassian.net/wiki/spaces/WEAVE/overview>

¹⁰<https://pfs.ipmu.jp/>

¹¹<https://www.asterochronometry.eu/haydn/>

¹²<http://jasmine.nao.ac.jp/index-en.html>

¹³<https://www.astro.lu.se/GaiaNIR>

¹⁴<https://www.skao.int/en>

¹⁵<https://ngvla.nrao.edu/>

Nacional / MCTI, The Ohio State University, Pennsylvania State University, Shanghai Astronomical Observatory, United Kingdom Participation Group, Universidad Nacional Autónoma de México, University of Arizona, University of Colorado Boulder, University of Oxford, University of Portsmouth, University of Utah, University of Virginia, University of Washington, University of Wisconsin, Vanderbilt University, and Yale University.

References

- Adibekyan VZ, Figueira P, Santos NC, Hakobyan AA, Sousa SG, Pace G, Delgado Mena E, Robin AC, Israelian G and González Hernández JI (2013), Jun. Kinematics and chemical properties of the Galactic stellar populations. The HARPS FGK dwarfs sample. *A&A* 554, A44. doi:10.1051/0004-6361/201321520. 1304.2561.
- Agertz O, Renaud F, Feltzing S, Read JI, Ryde N, Andersson EP, Rey MP, Bensby T and Feuillet DK (2021), Jun. VINTERGATAN - I. The origins of chemically, kinematically, and structurally distinct discs in a simulated Milky Way-mass galaxy. *MNRAS* 503 (4): 5826–5845. doi:10.1093/mnras/stab322. 2006.06008.
- Almannaei AS, Kawata D, Baba J, Hunt JAS, Seabroke G and Yan Z (2024), Apr. Impacts of the Local arm on the local circular velocity inferred from the Gaia DR3 young stars in the Milky Way. *MNRAS* 529 (2): 1035–1046. doi:10.1093/mnras/stae158. 2310.06831.
- Alves J, Zucker C, Goodman AA, Speagle JS, Meingast S, Robitaille T, Finkbeiner DP, Schlafly EF and Green GM (2020), Feb. A Galactic-scale gas wave in the solar neighbourhood. *Nature* 578 (7794): 237–239. doi:10.1038/s41586-019-1874-z. 2001.08748.
- Antoja T, Helmi A, Romero-Gómez M, Katz D, Babusiaux C, Drimmel R, Evans DW, Figueras F, Poggio E, Reylé C, Robin AC, Seabroke G and Soubiran C (2018), Sep. A dynamically young and perturbed Milky Way disk. *Nature* 561 (7723): 360–362. doi:10.1038/s41586-018-0510-7. 1804.10196.
- Antoja T, Ramos P, López-Guitart F, Anders F, Bernet M and Laporte CFP (2022), Dec. Tidally induced spiral arm wraps encoded in phase space. *A&A* 668, A61. doi:10.1051/0004-6361/202244064. 2206.03495.
- Antoja T, Ramos P, García-Conde B, Bernet M, Laporte CFP and Katz D (2023), May. The phase spiral in Gaia DR3. *A&A* 673, A115. doi:10.1051/0004-6361/202245518. 2212.11987.
- Asano T, Kawata D, Fujii MS and Baba J (2024), Mar. Growing local arm inferred by the breathing motion. *MNRAS* 529 (1): L7–L12. doi:10.1093/mnras/slzd190. 2310.02312.
- Asplund M, Amarsi AM and Grevesse N (2021), Sep. The chemical make-up of the Sun: A 2020 vision. *A&A* 653, A141. doi:10.1051/0004-6361/202140445. 2105.01661.
- Baba J and Kawata D (2020), Mar. Age dating the Galactic bar with the nuclear stellar disc. *MNRAS* 492 (3): 4500–4511. doi:10.1093/mnras/staa140. 1909.07548.
- Baba J, Kawata D and Schönrich R (2022), Jun. Age distribution of stars in boxy/peanut/X-shaped bulges formed without bar buckling. *MNRAS* 513 (2): 2850–2861. doi:10.1093/mnras/stac598. 2104.09526.
- Barros DA, Pérez-Villegas A, Lépine JRD, Michtchenko TA and Vieira RSS (2020), Jan. Exploring the Origin of Moving Groups and Diagonal Ridges by Simulations of Stellar Orbits and Birthplaces. *ApJ* 888 (2), 75. doi:10.3847/1538-4357/ab59d1. 1911.08675.
- Belokurov V and Kravtsov A (2022), Jul. From dawn till disc: Milky Way's turbulent youth revealed by the APOGEE+Gaia data. *MNRAS* 514 (1): 689–714. doi:10.1093/mnras/stac1267. 2203.04980.
- Belokurov V, Erkal D, Evans NW, Koposov SE and Deason AJ (2018), Jul. Co-formation of the disc and the stellar halo. *MNRAS* 478 (1): 611–619. doi:10.1093/mnras/sty982. 1802.03414.
- Belokurov V, Sanders JL, Fattahi A, Smith MC, Deason AJ, Evans NW and Grand RJJ (2020), May. The biggest splash. *MNRAS* 494 (3): 3880–3898. doi:10.1093/mnras/staa876. 1909.04679.
- Bennett M and Bovy J (2019), Jan. Vertical waves in the solar neighbourhood in Gaia DR2. *MNRAS* 482 (1): 1417–1425. doi:10.1093/mnras/sty2813. 1809.03507.
- Bennett M, Bovy J and Hunt JAS (2022), Mar. Exploring the Sgr-Milky Way-disk Interaction Using High-resolution N-body Simulations. *ApJ* 927 (1), 131. doi:10.3847/1538-4357/ac5021. 2107.08055.
- Bensby T, Feltzing S and Oey MS (2014), Feb. Exploring the Milky Way stellar disk. A detailed elemental abundance study of 714 F and G dwarf stars in the solar neighbourhood. *A&A* 562, A71. doi:10.1051/0004-6361/201322631. 1309.2631.
- Bergemann M, Sesar B, Cohen JG, Serenelli AM, Sheffield A, Li TS, Casagrande L, Johnston KV, Laporte CFP, Price-Whelan AM, Schönrich R and Gould A (2018), Mar. Two chemically similar stellar overdensities on opposite sides of the plane of the Galactic disk. *Nature* 555 (7696): 334–337. doi:10.1038/nature25490. 1803.00563.
- Binney J and Vasiliev E (2024), Jan. Chemodynamical models of our Galaxy. *MNRAS* 527 (2): 1915–1934. doi:10.1093/mnras/stad3312. 2306.11602.
- Bird JC, Kazantzidis S, Weinberg DH, Guedes J, Callegari S, Mayer L and Madau P (2013), Aug. Inside out and Upside down: Tracing the Assembly of a Simulated Disk Galaxy Using Mono-age Stellar Populations. *ApJ* 773 (1), 43. doi:10.1088/0004-637X/773/1/43. 1301.0620.
- Bland-Hawthorn J and Gerhard O (2016), Sep. The Galaxy in Context: Structural, Kinematic, and Integrated Properties. *ARA&A* 54: 529–596. doi:10.1146/annurev-astro-081915-023441. 1602.07702.
- Bland-Hawthorn J and Tepper-García T (2021), Jul. Galactic seismology: the evolving 'phase spiral' after the Sagittarius dwarf impact. *MNRAS* 504 (3): 3168–3186. doi:10.1093/mnras/stab704. 2009.02434.
- Blitz L and Spergel DN (1991), Oct. Direct Evidence for a Bar at the Galactic Center. *ApJ* 379: 631. doi:10.1086/170535.
- Bovy J (2015), Feb. galpy: A python Library for Galactic Dynamics. *ApJS* 216 (2), 29. doi:10.1088/0067-0049/216/2/29. 1412.3451.
- Bovy J, Rix HW, Liu C, Hogg DW, Beers TC and Lee YS (2012), Jul. The Spatial Structure of Mono-abundance Sub-populations of the Milky Way Disk. *ApJ* 753 (2), 148. doi:10.1088/0004-637X/753/2/148. 1111.1724.
- Bovy J, Leung HW, Hunt JAS, Mackereth JT, García-Hernández DA and Roman-Lopes A (2019), Dec. Life in the fast lane: a direct view of the dynamics, formation, and evolution of the Milky Way's bar. *MNRAS* 490 (4): 4740–4747. doi:10.1093/mnras/stz2891. 1905.11404.
- Brook CB, Kawata D, Gibson BK and Flynn C (2003), Mar. Galactic Halo Stars in Phase Space: A Hint of Satellite Accretion? *ApJL* 585 (2): L125–L129. doi:10.1086/374306. astro-ph/0301596.
- Brook CB, Kawata D, Gibson BK and Freeman KC (2004), Sep. The Emergence of the Thick Disk in a Cold Dark Matter Universe. *ApJ* 612 (2): 894–899. doi:10.1086/422709. astro-ph/0405306.
- Brook C, Richard S, Kawata D, Martel H and Gibson BK (2007), Mar. Two Disk Components from a Gas-Rich Disk-Disk Merger. *ApJ* 658 (1): 60–64. doi:10.1086/511056. astro-ph/0611748.
- Brook CB, Governato F, Roškar R, Stinson G, Brooks AM, Wadsley J, Quinn T, Gibson BK, Snaith O, Pilkington K, House E and Pontzen A

- (2011), Aug. Hierarchical formation of bulgeless galaxies: why outflows have low angular momentum. *MNRAS* 415 (2): 1051–1060. doi:10.1111/j.1365-2966.2011.18545.x. 1010.1004.
- Castro-Ginard A, McMillan PJ, Luri X, Jordi C, Romero-Gómez M, Cantat-Gaudin T, Casamiquela L, Tarricq Y, Soubiran C and Anders F (2021), Aug. Milky Way spiral arms from open clusters in Gaia EDR3. *A&A* 652, A162. doi:10.1051/0004-6361/202039751. 2105.04590.
- Chen X, Wang S, Deng L, de Grijs R, Liu C and Tian H (2019), Feb. An intuitive 3D map of the Galactic warp's precession traced by classical Cepheids. *Nature Astronomy* 3: 320–325. doi:10.1038/s41550-018-0686-7. 1902.00998.
- Chiba M and Beers TC (2000), Jun. Kinematics of Metal-poor Stars in the Galaxy. III. Formation of the Stellar Halo and Thick Disk as Revealed from a Large Sample of Nonkinematically Selected Stars. *AJ* 119 (6): 2843–2865. doi:10.1086/301409. astro-ph/0003087.
- Chiba R, Friske JKS and Schönrich R (2021), Jan. Resonance sweeping by a decelerating Galactic bar. *MNRAS* 500 (4): 4710–4729. doi:10.1093/mnras/staa3585. 1912.04304.
- Ciucă I, Kawata D, Miglio A, Davies GR and Grand RJJ (2021), May. Unveiling the distinct formation pathways of the inner and outer discs of the Milky Way with Bayesian Machine Learning. *MNRAS* 503 (2): 2814–2824. doi:10.1093/mnras/stab639. 2003.03316.
- Ciucă I, Kawata D, Ting YS, Grand RJJ, Miglio A, Hayden M, Baba J, Fragkoudi F, Monty S, Buder S and Freeman K (2024), Feb. Chasing the impact of the Gaia-Sausage-Enceladus merger on the formation of the Milky Way thick disc. *MNRAS* 528 (1): L122–L126. doi:10.1093/mnras/slud033. 2211.01006.
- Clarke JP and Gerhard O (2022), May. The pattern speed of the Milky Way bar/bulge from VIRAC and Gaia. *MNRAS* 512 (2): 2171–2188. doi:10.1093/mnras/stac603. 2107.10875.
- Colombo D, Duarte-Cabral A, Pettitt AR, Urquhart JS, Wyrowski F, Csengeri T, Neralwar KR, Schuller F, Menten KM, Anderson L, Barnes P, Beuther H, Bronfman L, Eden D, Ginsburg A, Henning T, König C, Lee MY, Mattern M, Medina S, Ragan SE, Rigby AJ, Sánchez-Monge Á, Traficante A, Yang AY and Wielen M (2022), Feb. The SEDIGISM survey: The influence of spiral arms on the molecular gas distribution of the inner Milky Way. *A&A* 658, A54. doi:10.1051/0004-6361/202141287. 2110.06071.
- Conroy C, Weinberg DH, Naidu RP, Buck T, Johnson JW, Cargile P, Bonaca A, Caldwell N, Chandra V, Han JJ, Johnson BD, Speagle JS, Ting YS, Woody T and Zaritsky D (2022), Apr. Birth of the Galactic Disk Revealed by the H3 Survey. *arXiv e-prints*, arXiv:2204.02989doi:10.48550/arXiv.2204.02989. 2204.02989.
- de Salas PF and Widmark A (2021), Oct. Dark matter local density determination: recent observations and future prospects. *Reports on Progress in Physics* 84 (10), 104901. doi:10.1088/1361-6633/ac24e7. 2012.11477.
- Deason AJ and Belokurov V (2024), Dec. Galactic Archaeology with Gaia. *New Astron. Rev.* 99, 101706. doi:10.1016/j.newar.2024.101706. 2402.12443.
- Debattista VP (2014), Sep. The vertical structure and kinematics of grand design spirals. *MNRAS* 443: L1–L5. doi:10.1093/mnras/slu069. 1405.6345.
- Dehnen W (1999), Oct. The Pattern Speed of the Galactic Bar. *ApJL* 524 (1): L35–L38. doi:10.1086/312299. astro-ph/9908105.
- Di Matteo P, Haywood M, Lehnert MD, Katz D, Khoperskov S, Snaith ON, Gómez A and Robichon N (2019), Dec. The Milky Way has no in-situ halo other than the heated thick disc. Composition of the stellar halo and age-dating the last significant merger with Gaia DR2 and APOGEE. *A&A* 632, A4. doi:10.1051/0004-6361/201834929. 1812.08232.
- Dobbs C and Baba J (2014), Sep. Dawes Review 4: Spiral Structures in Disc Galaxies. *PASA* 31, e035. doi:10.1017/pasa.2014.31. 1407.5062.
- Eggen OJ (1996), Oct. Star Streams and Galactic Structure. *AJ* 112: 1595. doi:10.1086/118126.
- Eggen OJ, Lynden-Bell D and Sandage AR (1962), Nov. Evidence from the motions of old stars that the Galaxy collapsed. *ApJ* 136: 748. doi:10.1086/147433.
- Eilers AC, Hogg DW, Rix HW, Frankel N, Hunt JAS, Fouvy JB and Buck T (2020), Sep. The Strength of the Dynamical Spiral Perturbation in the Galactic Disk. *ApJ* 900 (2), 186. doi:10.3847/1538-4357/abac0b. 2003.01132.
- Fragkoudi F, Katz D, Trick W, White SDM, Di Matteo P, Sormani MC, Khoperskov S, Haywood M, Hallé A and Gómez A (2019), Sep. On the ridges, undulations, and streams in Gaia DR2: linking the topography of phase space to the orbital structure of an N-body bar. *MNRAS* 488 (3): 3324–3339. doi:10.1093/mnras/stz1875. 1901.07568.
- Frankel N, Sanders J, Ting YS and Rix HW (2020), Jun. Keeping It Cool: Much Orbit Migration, yet Little Heating, in the Galactic Disk. *ApJ* 896 (1), 15. doi:10.3847/1538-4357/ab910c. 2002.04622.
- Friske JKS and Schönrich R (2019), Dec. More than just a wrinkle: a wave-like pattern in U_g versus L_z from Gaia data. *MNRAS* 490 (4): 5414–5423. doi:10.1093/mnras/stz2951. 1902.09569.
- Funakoshi N, Matsunaga N, Kawata D, Baba J, Taniguchi D and Fujii M (2024), Oct. Clues to growth and disruption of two neighbouring spiral arms of the Milky Way. *MNRAS* 533 (4): 4324–4333. doi:10.1093/mnras/stae2041. 2401.13037.
- Gaia Collaboration, Prusti T, de Bruijne JHJ, Brown AGA, Vallenari A, Babusiaux C, Bailer-Jones CAL, Bastian U, Biermann M, Evans DW, Eyer L, Jansen F, Jordi C, Klioner SA, Lammers U, Lindegren L, Luri X, Mignard F, Milligan DJ, Panem C, Poinsignon V, Pourbaix D, Randich S, Sarri G, Sartoretti P, Siddiqui HI, Soubiran C, Valette V, van Leeuwen F, Walton NA, Aerts C, Arenou F, Cropper M, Drimmel R, Hög E, Katz D, Lattanzi MG, O'Mullane W, Grebel EK, Holland AD, Huc C, Passot X, Bramante L, Cacciari C, Castañeda J, Chaoul L, Cheek N, De Angeli F, Fabricius C, Guerra R, Hernández J, Jean-Antoine-Piccolo A, Masana E, Messineo R, Mowlavi N, Nienartowicz K, Ordoñez-Blanco D, Panuzzo P, Portell J, Richards PJ, Riello M, Seabroke GM, Tanga P, Thévenin F, Torra J, Els SG, Gracia-Abril G, Comoretto G, García-Reinaldos M, Lock T, Mercier E, Altmann M, Andrae R, Astraatmadja TL, Bellas-Velidis I, Benson K, Berthier J, Blomme R, Busso G, Carry B, Cellino A, Clementini G, Cowell S, Creevey O, Cuypers J, Davidson M, De Ridder J, de Torres A, Delchambre L, Dell'Oro A, Ducourant C, Frémat Y, García-Torres M, Gossset E, Halbwegs JL, Hambly NC, Harrison DL, Hauser M, Hestroffer D, Hodgkin ST, Huckle HE, Hutton C, Jasiewicz G, Jordan S, Kontizas M, Korn AJ, Lanzafame AC, Manteiga M, Moitinho A, Muinonen K, Osinde J, Pancino E, Pauwels T, Petit JM, Recio-Blanco A, Robin AC, Sarro LM, Siopis C, Smith M, Smith KW, Sozzetti A, Thuillot W, van Reeven W, Viala Y, Abbas U, Abreu Aramburu A, Accart S, Aguado JJ, Allan PM, Allasia W, Altavilla G, Álvarez MA, Alves J, Anderson RI, Andrei AH, Anglada Varela E, Antiche E, Antoja T, Antón S, Arcay B, Atzei A, Ayache L, Bach N, Baker SG, Balaguer-Núñez L, Barache C, Barata C, Barbier A, Barblan F, Baroni M, Barrado y Navascués D, Barros M, Barstow MA, Becciani U, Bellazzini M, Bellei G, Bello García A, Belokurov V, Bendjoya P, Berihuete A, Bianchi L, Bienaymé O, Billebaud F, Blagorodnova N, Blanco-Cuaresma S, Boch T, Bombrun A, Borrachero R, Bouquillon S, Bourda G, Bouy H, Bragaglia A, Breddels MA, Brouillet N, Brùsemeister T, Bucciarelli B, Budnik F, Burgess P, Burgon R, Burlacu A, Busonero D, Buzzi R, Caffau E, Cambras J, Campbell H, Cancelliere R, Cantat-Gaudin T, Carracci T, Carrasco JM, Castellani M, Charlot P, Charnas J, Charvet P, Chassat F, Chiavassa A, Clotet M, Cocozza G, Collins RS, Collins P, Costigan G, Crifo F, Cross NJG, Crosta M, Crowley C, Dafonte C, Damerdjij Y, Dapergolas A, David P, David M, De Cat P, de Felice F, de Laverny P, De Luise F, De March R, de Martino D, de Souza R, Debusscher J, del Pozo E, Delbo M, Delgado A, Delgado HE, di Marco F, Di Matteo P, Diakite S, Distefano E, Dolding C, Dos Anjos S, Drazinos P, Durán J, Dzigan Y, Ecale E, Edvardsson B, Enke H, Erdmann M, Escolar T, Espina M, Evans NW, Eynard Bontemps G, Fabre C, Fabrizio M, Faigler S, Falcão AJ, Farràs Casas M, Faye F, Federici L, Fedorets G, Fernández-Hernández J, Fernique P, Fienga A, Figueras F, Filippi F, Findelsen K, Fonti A, Fouesneau M, Fraile E, Fraser M, Fuchs J, Furnell R, Gai M, Galletti S, Galluccio L, Garabato D, García-Sedano F, Garé P, Garofalo A, Garralda N, Gavras P, Gerssen J, Geyer R, Gilmore G, Girona S, Giuffrida G, Gomes M, González-Marcos A, González-Núñez

J, González-Vidal JJ, Granvik M, Guerrier A, Guillout P, Guiraud J, Gúrpide A, Gutiérrez-Sánchez R, Guy LP, Haigron R, Hatzidimitriou D, Haywood M, Heiter U, Helmi A, Hobbs D, Hofmann W, Holl B, Holland G, Hunt JAS, Hypki A, Icardi V, Irwin M, Jevardat de Fombelle G, Jofré P, Jonker PG, Jorissen A, Julbe F, Karampelas A, Kochoska A, Kohley R, Kolenberg K, Kontizas E, Koposov SE, Kordopatis G, Koubisy P, Kowalczyk A, Krone-Martins A, Kudryashova M, Kull I, Bachchan RK, Lacoste-Seris F, Lanza AF, Lavigne JB, Le Poncin-Lafitte C, Lebreton Y, Lebzelter T, Leccia S, Leclerc N, Lecoœur-Taibi I, Lemaître V, Lenhardt H, Leroux F, Liao S, Licata E, Lindström HEP, Lister TA, Livanou E, Lobel A, Löffler W, López M, Lopez-Lozano A, Lorenz D, Loureiro T, MacDonald I, Magalhães Fernandes T, Managau S, Mann RG, Mantelet G, Marchal O, Marchant JM, Marconi M, Marie J, Marinoni S, Marrese PM, Marschalkó G, Marshall DJ, Martín-Fleitas JM, Martino M, Mary N, Matijević G, Mazeh T, McMillan PJ, Messina S, Mestre A, Michalik D, Millar NR, Miranda BMH, Molina D, Molinaro R, Molinaro M, Molnár L, Moniez M, Montegriffo P, Monteiro D, Mor R, Mora A, Morbidelli R, Morel T, Morgenthaler S, Morley T, Morris D, Mulone AF, Muraveva T, Musella I, Narbonne J, Nelemans G, Nicastro L, Noval L, Ordénovic C, Ordieres-Meré J, Osborne P, Pagani C, Pagano I, Pailler F, Palacin H, Palaversa L, Parsons P, Paulsen T, Pecoraro M, Pedrosa R, Pentikäinen H, Pereira J, Pichon B, Piersimoni AM, Pineau FX, Plachy E, Plum G, Poujoulet E, Prša A, Pulone L, Ragaini S, Rago S, Rambaux N, Ramos-Lerate M, Ranalli P, Rauw G, Read A, Regibo S, Renk F, Reylé C, Ribeiro RA, Rimoldini L, Ripepi V, Riva A, Rixon G, Roelens M, Romero-Gómez M, Rowell N, Royer F, Rudolph A, Ruiz-Dern L, Sadowski G, Sagristà Sellés T, Sahlmann J, Salgado J, Salguero E, Sarasso M, Savietto H, Schnorhk A, Schultheis M, Sciacca E, Segol M, Segovia JC, Segransan D, Serpell E, Shih IC, Smareglia R, Smart RL, Smith C, Solano E, Solitto F, Sordo R, Soria Nieto S, Souchay J, Spagna A, Spoto F, Stampa U, Steele IA, Steidelmüller H, Stephenson CA, Stoev H, Suess FF, Süveges M, Surdej J, Szabados L, Szegedi-Elek E, Tapiador D, Taris F, Tauran G, Taylor MB, Teixeira R, Terrett D, Tingley R, Trager SC, Turon C, Ulla A, Utrilla E, Valentini G, van Elteren A, Van Hemelryck E, van Leeuwen M, Varadi M, Vecchiato A, Veljanoski J, Via T, Vicente D, Vogt S, Voss H, Votruba V, Voutsinas S, Walmsley G, Weiler M, Weingrill K, Werner D, Wevers T, Whitehead G, Wyrzykowski Ł, Yoldas A, Žerjal M, Zucker S, Zurbach C, Zwitter T, Alecu A, Allen M, Allende Prieto C, Amorim A, Anglada-Escudé G, Arsenijević V, Azas S, Balm P, Beck M, Bernstein HH, Bigot L, Bijaoui A, Blasco C, Bonfigli M, Bono G, Boudreault S, Bressan A, Brown S, Brunet PM, Bunclark P, Buonanno R, Butkevich AG, Carret C, Carrion C, Chemin L, Chéreau F, Corcione L, Darmigny E, de Boer KS, de Teodoro P, de Zeeuw PT, Delle Luche C, Domingues CD, Dubath P, Fodor F, Frézouls B, Fries A, Fustes D, Fyfe D, Gallardo E, Gallegos J, Gardiol D, Gebran M, Gomboc A, Gómez A, Grux E, Gueguen A, Heyrovsky A, Hoar J, Iannicola G, Isasi Parache Y, Janotto AM, Joliet E, Jonckheere A, Keil R, Kim DW, Klagyivik P, Klar J, Knude J, Kochukhov O, Kolka I, Kos J, Kutka A, Lainey V, LeBouquin D, Liu C, Loreggia D, Makarov VV, Marseille MG, Martayan C, Martínez-Rubi O, Massart B, Meynadier F, Mignot S, Munari U, Nguyen AT, Nordlander T, Ocvirk P, O'Flaherty KS, Olias Sanz A, Ortiz P, Osorio J, Oszkiewicz D, Ouzounis A, Palmer M, Park P, Pasquato E, Peltzer C, Peralta J, Péturaud F, Pieniluoma T, Pigozzi E, Poels J, Prat G, Prod'homme T, Raison F, Rebordao JM, Riskey D, Rocca-Volmerange B, Rosen S, Ruiz-Fuertes MI, Russo F, Sembay S, Serraller Vizcaino I, Short A, Siebert A, Silva H, Sinachopoulos D, Slezak E, Soffel M, Sosnowska D, Straizys V, ter Linden M, Terrell D, Theil S, Tiede C, Troisi L, Tsalmantza P, Tur D, Vaccari M, Vachier F, Valles P, Van Hamme W, Veltz L, Virtanen J, Wallut JM, Wichmann R, Wilkinson MI, Ziaeeppour H and Zschocke S (2016), *Nov. The Gaia mission*. *A&A* 595, A1. doi:10.1051/0004-6361/201629272. 1609.04153.

Gaia Collaboration, Vallenari A, Brown AGA, Prusti T, de Bruijne JHJ, Arenou F, Babusiaux C, Biermann M, Creevey OL, Ducourant C, Evans DW, Eyer L, Guerra R, Hutton A, Jordi C, Klioner SA, Lammas UL, Lindegren L, Luri X, Mignard F, Panem C, Pourbaix D, Randich S, Sartoretti P, Soubiran C, Tanga P, Walton NA, Bailer-Jones CAL, Bastian U, Drimmel R, Jansen F, Katz D, Lattanzi MG, van Leeuwen F, Bakker J, Cacciari C, Castañeda J, De Angeli F, Fabricius C, Fouesneau M, Frémat Y, Galluccio L, Guerrier A, Heiter U, Masana E, Messineo R, Mowlavi N, Nicolas C, Nienartowicz K, Pailler F, Panuzzo P, Riclet F, Roux W, Seabroke GM, Sordo R, Thévenin F, Gracia-Abril G, Portell J, Teyssier D, Aitmann M, Andrae R, Audard M, Bellas-Verdís I, Benson K, Berthier J, Blomme R, Burgess PW, Busonero D, Busso G, Cánovas H, Carry B, Cellino A, Cheek N, Clementini G, Damerdji Y, Davidson M, de Teodoro P, Nuñez Campos M, Delchambre L, Dell'Oro A, Esquej P, Fernández-Hernández J, Fraile E, Garabato D, García-Lario P, Gosset E, Haigron R, Halbwegs JL, Hambly NC, Harrison DL, Hernández J, Hestroffer D, Hodgkin ST, Holl B, Janßen K, Jevardat de Fombelle G, Jordan S, Krone-Martins A, Lanzafame AC, Löffler W, Marchal O, Marrese PM, Moitinho A, Muinonen K, Osborne P, Pancino E, Pauwels T, Recio-Blanco A, Reylé C, Riello M, Rimoldini L, Roegiers T, Rybizki J, Sarro LM, Siopis C, Smith M, Sozzetti A, Utrilla E, van Leeuwen M, Abbas U, Ábrahám P, Abreu Aramburu A, Aerts C, Aguado JJ, Ajaj M, Aldea-Montero F, Altavilla G, Álvarez MA, Alves J, Anders F, Anderson RI, Anglada Varela E, Antoja T, Baines D, Baker SG, Balaguer-Núñez L, Balbinot E, Balog Z, Barache C, Barbato D, Barros M, Barstow MA, Bartolomé S, Bassilana JL, Bauchet N, Becciani U, Bellazzini M, Berihuete A, Bernet M, Bertone S, Bianchi L, Binnerfeld A, Blanco-Cuaresma S, Blazere A, Boch T, Bombrun A, Bossini D, Bouquillon S, Bragaglia A, Bramante L, Breedt E, Bressan A, Brouillet N, Brugaletta E, Bucciarelli B, Burlacu A, Butkevich AG, Buzzzi R, Caffau E, Cancelliere R, Cantat-Gaudin T, Carballo R, Carlucci T, Carnerero MI, Carrasco JM, Casamiquela L, Castellani M, Castro-Ginard A, Chaoul L, Charlot P, Chemin L, Chiaramida V, Chiavassa A, Chornay N, Comoretto G, Contursi G, Cooper WJ, Cornez T, Cowell S, Crifo F, Cropper M, Crosta M, Crowley C, Dafonte C, Daperolas A, David M, David P, de Laverny P, De Luise F, De March R, De Ridder J, de Souza R, de Torres A, del Peloso EF, del Pozo E, Delbo M, Delgado A, Delisle JB, Demouchy C, Dharmawardena TE, Di Matteo P, Diakite S, Diener C, Distefano E, Dolding C, Edvardsson B, Enke H, Fabre C, Fabrizio M, Faigler S, Fedorets G, Fernique P, Fienga A, Figueras F, Fournier Y, Fouron C, Fragkoudi F, Gai M, Garcia-Gutierrez A, Garcia-Reinaldos M, Garcia-Torres M, Garofalo A, Gavel A, Gavras P, Gerlach E, Geyer R, Giacobbe P, Gilmore G, Girona S, Giuffrida G, Gommel R, Gomez A, González-Núñez J, González-Santamaría I, González-Vidal JJ, Granvik M, Guillout P, Guiraud J, Gutiérrez-Sánchez R, Guy LP, Hatzidimitriou D, Hauser M, Haywood M, Helmer A, Helmi A, Helmi A, Sarmiento MH, Hidalgo SL, Hilger T, Hładczuk N, Hobbs D, Holland G, Huckle HE, Jardine K, Jasiewicz G, Jean-Antoine Piccolo A, Jiménez-Arranz Ó, Jorissen A, Juaristi Campillo J, Julbe F, Karbevská L, Kervella P, Khanna S, Kontizas M, Kordopatis G, Korn AJ, Kóspál Á, Kostrzewa-Rutkowska Z, Kruszyńska K, Kun M, Laizeau P, Lambert S, Lanza AF, Lasne Y, Le Campion JF, Lebreton Y, Lebzelter T, Leccia S, Leclerc N, Lecoœur-Taibi I, Liao S, Licata EL, Lindström HEP, Lister TA, Livanou E, Lobel A, Lorca A, Loup C, Madrero Pardo P, Magdalena Romeo A, Managau S, Mann RG, Manteiga M, Marchant JM, Marconi M, Marcos J, Marcos Santos MMS, Marín Pina D, Marinoni S, Marocco F, Marshall DJ, Martín Polo L, Martín-Fleitas JM, Marton G, Mary N, Masip A, Massari D, Mastrobuono-Battisti A, Mazeh T, McMillan PJ, Messina S, Michalik D, Millar NR, Mints A, Molina D, Molinaro R, Molnár L, Monari G, Monguió M, Montegriffo P, Montero A, Mor R, Mora A, Morbidelli R, Morel T, Morris D, Muraveva T, Murphy CP, Musella I, Nagy Z, Noval L, Ocaña F, Ogden A, Ordenovic C, Osinde JO, Pagani C, Pagano I, Palaversa L, Palicio PA, Pallas-Quintela L, Panahi A, Payne-Wardenaar S, Peñalosa Esteller X, Penttilä A, Pichon B, Piersimoni AM, Pineau FX, Plachy E, Plum G, Poggio E, Prša A, Pulone L, Racero E, Ragaini S, Rainer M, Raiteri CM, Rambaux N, Ramos P, Ramos-Lerate M, Re Fiorentin P, Regibo S, Richards PJ, Rios Diaz C, Ripepi V, Riva A, Rix HW, Rixon G, Robichon N, Robin AC, Robin C, Roelens M, Rogues HRO, Rohrbasser L, Romero-Gómez M, Rowell N, Royer F, Ruz Mieres D, Rybizki KA, Sadowski G, Sáez Núñez A, Sagristà Sellés A, Sahlmann J, Salguero E, Samaras N, Sanchez Gimenez V, Sanna N, Santoveña R, Sarasso M, Schultheis M, Sciacca E, Segol M, Segovia JC, Ségransan D, Semeux D, Shahaf S, Siddiqui HI, Siebert A, Siltala L, Silvelo A, Slezak E, Slezak I, Smart RL, Snaith ON, Solano E, Solitto F, Souami D, Souchay J, Spagna A, Spina L, Spoto F, Steele IA, Steidelmüller H, Stephenson CA, Süveges M, Surdej J, Szabados L, Szegedi-Elek E, Taris F, Taylor MB, Teixeira R, Tolomei L, Tonello N, Torra F, Torra F, Torralba Elipe G, Trabucchi M, Tsounis AT, Turon C, Ulla A, Unger N, Vaillant MV, van Dillen E, van Reeve W, Vanel O, Vecchiato A, Viala Y, Vicente D, Voutsinas S, Weiler M, Wevers T, Wyrzykowski Ł, Yoldas A, Yvard P, Zhao H, Zorec J, Zucker S and Zwitter T (2023), *Jun. Gaia Data Release 3. Summary of the content and survey properties*. *A&A* 674, A1. doi:10.1051/0004-6361/202243940. 2208.00211.

- Gallart C, Bernard EJ, Brook CB, Ruiz-Lara T, Cassisi S, Hill V and Monelli M (2019), Jul. Uncovering the birth of the Milky Way through accurate stellar ages with Gaia. *Nature Astronomy* 3: 932–939. doi:10.1038/s41550-019-0829-5. 1901.02900.
- Gilmore G and Reid N (1983), Mar. New light on faint stars - III. Galactic structure towards the South Pole and the Galactic thick disc. *MNRAS* 202: 1025–1047. doi:10.1093/mnras/202.4.1025.
- Grand RJJ, Kawata D and Cropper M (2012), Apr. The dynamics of stars around spiral arms. *MNRAS* 421 (2): 1529–1538. doi:10.1111/j.1365-2966.2012.20411.x. 1112.0019.
- Grand RJJ, Bustamante S, Gómez FA, Kawata D, Marinacci F, Pakmor R, Rix HW, Simpson CM, Sparre M and Springel V (2018), Mar. Origin of chemically distinct disks in the Auriga cosmological simulations. *MNRAS* 474 (3): 3629–3639. doi:10.1093/mnras/stx3025. 1708.07834.
- Grand RJJ, Kawata D, Belokurov V, Deason AJ, Fattahi A, Fragkoudi F, Gómez FA, Marinacci F and Pakmor R (2020), Sep. The dual origin of the Galactic thick disc and halo from the gas-rich Gaia-Enceladus Sausage merger. *MNRAS* 497 (2): 1603–1618. doi:10.1093/mnras/staa2057. 2001.06009.
- Grand RJJ, Pakmor R, Fragkoudi F, Gómez FA, Trick W, Simpson CM, van de Voort F and Bieri R (2023), Sep. An ever-present Gaia snail shell triggered by a dark matter wake. *MNRAS* 524 (1): 801–816. doi:10.1093/mnras/stad1969. 2211.08437.
- GRAVITY Collaboration, Abuter R, Amorim A, Bauböck M, Berger JP, Bonnet H, Brandner W, Clénet Y, Davies R, de Zeeuw PT, Dexter J, Dillal Y, Drescher A, Eckart A, Eisenhauer F, Förster Schreiber NM, García P, Gao F, Gendron E, Genzel R, Gillessen S, Habibi M, Haubois X, Heißel G, Henning T, Hippler S, Horrobin M, Jiménez-Rosales A, Jochum L, Jocu L, Kaufer A, Kervella P, Lacour S, Lapeyrière V, Le Bouquin JB, Léna P, Lutz D, Nowak M, Ott T, Paumard T, Perraut K, Perrin G, Pfuhl O, Rabien S, Rodríguez-Coira G, Shangqun G, Shimizu T, Scheithauer S, Stadler J, Straub O, Straubmeier C, Sturm E, Tacconi LJ, Vincent F, von Fellenberg S, Waisberg I, Widmann F, Wieprecht E, Wiezorrek E, Woillez J, Yazici S, Young A and Zins G (2021), Mar. Improved GRAVITY astrometric accuracy from modeling optical aberrations. *A&A* 647, A59. doi:10.1051/0004-6361/202040208. 2101.12098.
- Hayden MR, Bovy J, Holtzman JA, Nidever DL, Bird JC, Weinberg DH, Andrews BH, Majewski SR, Allende Prieto C, Anders F, Beers TC, Bizyaev D, Chiappini C, Cunha K, Frinchaboy P, García-Hernández DA, García Pérez AE, Girardi L, Harding P, Hearty FR, Johnson JA, Mészáros S, Minchev I, O’Connell R, Pan K, Robin AC, Schiavon RP, Schneider DP, Schultheis M, Shetrone M, Skrutskie M, Steinmetz M, Smith V, Wilson JC, Zamora O and Zasowski G (2015), Aug. Chemical Cartography with APOGEE: Metallicity Distribution Functions and the Chemical Structure of the Milky Way Disk. *ApJ* 808 (2), 132. doi:10.1088/0004-637X/808/2/132. 1503.02110.
- Haywood M, Di Matteo P, Lehnert MD, Snaith O, Khoperskov S and Gómez A (2018), Aug. In Disguise or Out of Reach: First Clues about In Situ and Accreted Stars in the Stellar Halo of the Milky Way from Gaia DR2. *ApJ* 863 (2), 113. doi:10.3847/1538-4357/aad235. 1805.02617.
- Haywood M, Snaith O, Lehnert MD, Di Matteo P and Khoperskov S (2019), May. Revisiting long-standing puzzles of the Milky Way: the Sun and its vicinity as typical outer disk chemical evolution. *A&A* 625, A105. doi:10.1051/0004-6361/201834155. 1903.03188.
- Helmi A, Babusiaux C, Koppelman HH, Massari D, Veljanoski J and Brown AGA (2018), Nov. The merger that led to the formation of the Milky Way’s inner stellar halo and thick disk. *Nature* 563 (7729): 85–88. doi:10.1038/s41586-018-0625-x. 1806.06038.
- Hobbs D, Brown A, Høg E, Jordi C, Kawata D, Tanga P, Klioner S, Sozzetti A, Wyrzykowski Ł, Walton N, Vallenari A, Makarov V, Rybizki J, Jiménez-Esteban F, Caballero JA, McMillan PJ, Seccrest N, Mor R, Andrews JJ, Zwitter T, Chiappini C, Fynbo JPU, Ting YS, Hestroffer D, Lindegren L, McArthur B, Gouda N, Moore A, Gonzalez OA and Vaccari M (2021), Jun. All-sky visible and near infrared space astrometry. *Experimental Astronomy* 51 (3): 783–843. doi:10.1007/s10686-021-09705-z. 1907.12535.
- Hou LG (2021), Aug. The spiral structure in the Solar neighbourhood. *Frontiers in Astronomy and Space Sciences* 8, 103. doi:10.3389/fspas.2021.671670. 2110.04446.
- Howard CD, Rich RM, Reitzel DB, Koch A, De Propriis R and Zhao H (2008), Dec. The Bulge Radial Velocity Assay (BRAVA). I. Sample Selection and a Rotation Curve. *ApJ* 688 (2): 1060–1077. doi:10.1086/592106. 0807.3967.
- Hu S and Sijacki D (2016), Sep. Stellar spiral structures in triaxial dark matter haloes. *MNRAS* 461 (3): 2789–2808. doi:10.1093/mnras/stw1463. 1507.01643.
- Hunt JAS and Bovy J (2018), Jul. The 4:1 outer Lindblad resonance of a long-slow bar as an explanation for the Hercules stream. *MNRAS* 477 (3): 3945–3953. doi:10.1093/mnras/sty921. 1803.02358.
- Hunt JAS and Vasiliev E (2024), Dec. Milky Way dynamics in light of Gaia. *New Astron. Rev.* submitted.
- Hunt JAS, Hong J, Bovy J, Kawata D and Grand RJJ (2018), Dec. Transient spiral structure and the disc velocity substructure in Gaia DR2. *MNRAS* 481 (3): 3794–3803. doi:10.1093/mnras/sty2532. 1806.02832.
- Hunt JAS, Bub MW, Bovy J, Mackereth JT, Trick WH and Kawata D (2019), Nov. Signatures of resonance and phase mixing in the Galactic disc. *MNRAS* 490 (1): 1026–1043. doi:10.1093/mnras/stz2667. 1904.10968.
- Hunt JAS, Price-Whelan AM, Johnston KV and Darragh-Ford E (2022), Oct. Multiple phase spirals suggest multiple origins in Gaia DR3. *MNRAS* 516 (1): L7–L11. doi:10.1093/mnras/516/1/L7. 2206.06125.
- Hunt JAS, Price-Whelan AM, Johnston KV, McClure RL, Filion C, Cassese B and Horta D (2024), Feb. Radial phase spirals in the Solar neighbourhood. *MNRAS* 527 (4): 11393–11403. doi:10.1093/mnras/stad3918. 2401.08748.
- Imig J, Price C, Holtzman JA, Stone-Martinez A, Majewski SR, Weinberg DH, Johnson JA, Allende Prieto C, Beaton RL, Beers TC, Bizyaev D, Blanton MR, Brownstein JR, Cunha K, Fernández-Trincado JG, Feuillet DK, Hasselquist S, Hayes CR, Jönsson H, Lane RR, Lian J, Mészáros S, Nidever DL, Robin AC, Shetrone M, Smith V and Wilson JC (2023), Sep. A Tale of Two Disks: Mapping the Milky Way with the Final Data Release of APOGEE. *ApJ* 954 (2), 124. doi:10.3847/1538-4357/ace9b8. 2307.13887.
- Jeans JH (1922), Jan. The Motions of Stars in a Kapteyn Universe. *MNRAS* 82: 122–132. doi:10.1093/mnras/82.3.122.
- Jurić M, Ivezić Ž, Brooks A, Lupton RH, Schlegel D, Finkbeiner D, Padmanabhan N, Bond N, Sesar B, Rockosi CM, Knapp GR, Gunn JE, Sumi T, Schneider DP, Barentine JC, Brewington HJ, Brinkmann J, Fukugita M, Harvanek M, Kleinman SJ, Krzesinski J, Long D, Neilsen Eric H. J, Nitta A, Snedden SA and York DG (2008), Feb. The Milky Way Tomography with SDSS. I. Stellar Number Density Distribution. *ApJ* 673 (2): 864–914. doi:10.1086/523619. astro-ph/0510520.
- Kalnajs AJ (1973), Oct. Spiral Structure Viewed as a Density Wave. *PASA* 2 (4): 174–177. doi:10.1017/S132335800013461.
- Kapteyn JC (1922), May. First Attempt at a Theory of the Arrangement and Motion of the Sidereal System. *ApJ* 55: 302. doi:10.1086/142670.
- Kawata D and Chiappini C (2016), Sep. Milky Way’s thick and thin disk: Is there a distinct thick disk? *Astronomische Nachrichten* 337 (8-9): 976. doi:10.1002/asna.201612421. 1608.01698.
- Kawata D, Baba J, Ciucă I, Cropper M, Grand RJJ, Hunt JAS and Seabroke G (2018), Sep. Radial distribution of stellar motions in Gaia DR2. *MNRAS* 479 (1): L108–L112. doi:10.1093/mnras/sly107. 1804.10175.
- Kawata D, Kawahara H, Gouda N, Seccrest NJ, Kano R, Kataya H, Isobe N, Ohsawa R, Usui F, Yamada Y, Graham AW, Pettitt AR, Asada H, Baba J, Bekki K, Dorland BN, Fujii M, Fukui A, Hattori K, Hirano T, Kamizuka T, Kashima S, Kawanaka N, Kawashima Y, Klioner SA, Kodama T, Koshimoto N, Kotani T, Kuzuhara M, Levine SE, Majewski SR, Masuda K, Matsunaga N, Miyakawa K, Miyoshi M, Morihana K, Nishi R, Notsu Y, Omiya M, Sanders J, Tanikawa A, Tsujimoto M, Yano T, Aizawa M, Arimatsu K, Biermann M, Boehm C, Chiba M, Debattista VP, Gerhard O, Hirabayashi M, Hobbs D, Ikenoue B, Izumiura H, Jordi C, Kohara N, Löffler W, Luri X, Mase I, Miglio A, Mitsuda K, Newswander T, Nishiyama S, Obuchi Y, Ootsubo T, Ouchi M, Ozaki M, Perryman M, Prusti T, Ramos P, Read JI, Rich RM, Schönrich R, Shikauchi M,

- Shimizu R, Suematsu Y, Tada S, Takahashi A, Tatekawa T, Tatsumi D, Tsujimoto T, Tsuzuki T, Urakawa S, Uruguchi F, Utsunomiya S, Van Eylen V, van Leeuwen F, Wada T and Walton NA (2024), Jun. JASMIN: Near-infrared astrometry and time-series photometry science. *PASJ* 76 (3): 386–425. doi:10.1093/pasj/psae020. 2307.05666.
- Kereš D, Katz N, Weinberg DH and Davé R (2005), Oct. How do galaxies get their gas? *MNRAS* 363 (1): 2–28. doi:10.1111/j.1365-2966.2005.09451.x. astro-ph/0407095.
- Khoperskov S, Di Matteo P, Gerhard O, Katz D, Haywood M, Combes F, Berczik P and Gomez A (2019), Feb. The echo of the bar buckling: Phase-space spirals in Gaia Data Release 2. *A&A* 622, L6. doi:10.1051/0004-6361/201834707. 1811.09205.
- Kobayashi C, Karakas AI and Lugaro M (2020), Sep. The Origin of Elements from Carbon to Uranium. *ApJ* 900 (2), 179. doi:10.3847/1538-4357/abac65. 2008.04660.
- Laporte CFP, Minchev I, Johnston KV and Gómez FA (2019), May. Footprints of the Sagittarius dwarf galaxy in the Gaia data set. *MNRAS* 485 (3): 3134–3152. doi:10.1093/mnras/stz583. 1808.00451.
- Lian J, Zasowski G, Chen B, Imig J, Wang T, Boardman N and Liu X (2024), Jun. The broken-exponential radial structure and larger size of the Milky Way galaxy. *Nature Astronomy* doi:10.1038/s41550-024-02315-7. 2406.05604.
- Licquia TC and Newman JA (2016), Nov. Sizing Up the Milky Way: A Bayesian Mixture Model Meta-analysis of Photometric Scale Length Measurements. *ApJ* 831 (1), 71. doi:10.3847/0004-637X/831/1/71. 1607.05281.
- Lin CC and Shu FH (1964), Aug. On the Spiral Structure of Disk Galaxies. *ApJ* 140: 646. doi:10.1086/147955.
- Lin X, Xu Y, Hou L, Liu D, Li Y, Hao C, Li J and Bian S (2022), May. Local Spiral Structure Traced by Red Clump Stars. *ApJ* 931 (1), 72. doi:10.3847/1538-4357/ac67a6. 2205.15507.
- Majewski SR, Schiavon RP, Frinchaboy PM, Allende Prieto C, Barkhouser R, Bizyaev D, Blank B, Brunner S, Burton A, Carrera R, Chojnowski SD, Cunha K, Epstein C, Fitzgerald G, García Pérez AE, Hearty FR, Henderson C, Holtzman JA, Johnson JA, Lam CR, Lawler JE, Maseman P, Mészáros S, Nelson M, Nguyen DC, Nidever DL, Pinsonneault M, Shetrone M, Smee S, Smith VV, Stolberg T, Skrutskie MF, Walker E, Wilson JC, Zasowski G, Anders F, Basu S, Beland S, Blanton MR, Bovy J, Brownstein JR, Carlberg J, Chaplin W, Chiappini C, Eisenstein DJ, Elsworth Y, Feuillet D, Fleming SW, Galbraith-Frew J, García RA, García-Hernández DA, Gillespie BA, Girardi L, Gunn JE, Hasselquist S, Hayden MR, Hekker S, Ivans I, Kinemuchi K, Klaene M, Mahadevan S, Mathur S, Mosser B, Muna D, Munn JA, Nichol RC, O’Connell RW, Parejko JK, Robin AC, Rocha-Pinto H, Schultheis M, Serenelli AM, Shane N, Silva Aguirre V, Sobek JS, Thompson B, Troup NW, Weinberg DH and Zamora O (2017), Sep. The Apache Point Observatory Galactic Evolution Experiment (APOGEE). *AJ* 154 (3), 94. doi:10.3847/1538-3881/aa784d. 1509.05420.
- Mason AC, Crain RA, Schiavon RP, Weinberg DH, Pfeffer J, Schaye J, Schaller M and Theuns T (2024), Sep. Realistic simulated galaxies form $[\alpha/\text{Fe}]$ - $[\text{Fe}/\text{H}]$ knees due to a sustained decline in their star formation rates. *MNRAS* 533 (1): 184–200. doi:10.1093/mnras/stae1743. 2311.00041.
- McMillan PJ (2017), Feb. The mass distribution and gravitational potential of the Milky Way. *MNRAS* 465 (1): 76–94. doi:10.1093/mnras/stw2759. 1608.00971.
- McWilliam A and Zoccali M (2010), Dec. Two Red Clumps and the X-shaped Milky Way Bulge. *ApJ* 724 (2): 1491–1502. doi:10.1088/0004-637X/724/2/1491. 1008.0519.
- Morrow A, Grand RJJ, Fragkoudi F and Martig M (2024), Jun. Did the Gaia Enceladus/Sausage merger form the Milky Way’s bar? *MNRAS* 531 (1): 1520–1533. doi:10.1093/mnras/stae1250. 2312.02318.
- Miglio A, Chiappini C, Mackereth JT, Davies GR, Brogaard K, Casagrande L, Chaplin WJ, Girardi L, Kawata D, Khan S, Izzard R, Montalbán J, Mosser B, Vincenzo F, Bossini D, Noels A, Rodrigues T, Valentini M and Mandel I (2021a), Jan. Age dissection of the Milky Way discs: Red giants in the Kepler field. *A&A* 645, A85. doi:10.1051/0004-6361/202038307. 2004.14806.
- Miglio A, Girardi L, Grundahl F, Mosser B, Bastian N, Bragaglia A, Brogaard K, Buldgen G, Chantereau W, Chaplin W, Chiappini C, Dupret MA, Eggenberger P, Gieles M, Izzard R, Kawata D, Karoff C, Lagarde N, Mackereth T, Magrin D, Meynet G, Michel E, Montalbán J, Nascimbeni V, Noels A, Piotto G, Ragazzoni R, Soszyński I, Tolstoy E, Toonen S, Triaud A and Vincenzo F (2021b), Jun. Haydn. *Experimental Astronomy* 51 (3): 963–1001. doi:10.1007/s10686-021-09711-1. 1908.05129.
- Minchev I, Anders F, Recio-Blanco A, Chiappini C, de Laverny P, Queiroz A, Steinmetz M, Adibekyan V, Carrillo I, Cescutti G, Guiglion G, Hayden M, de Jong RS, Kordopatis G, Majewski SR, Martig M and Santiago BX (2018), Dec. Estimating stellar birth radii and the time evolution of Milky Way’s ISM metallicity gradient. *MNRAS* 481 (2): 1645–1657. doi:10.1093/mnras/sty2033. 1804.06856.
- Nakada Y, Onaka T, Yamamura I, Deguchi S, Hashimoto O, Izumiura H and Sekiguchi K (1991), Sep. Is the bulge of our Galaxy triaxial? *Nature* 353 (6340): 140–141. doi:10.1038/353140a0.
- Nakanishi H and Sofue Y (2016), Feb. Three-dimensional distribution of the ISM in the Milky Way galaxy. III. The total neutral gas disk. *PASJ* 68 (1), 5. doi:10.1093/pasj/psv108. 1511.08877.
- Nissen PE and Schuster WJ (2010), Feb. Two distinct halo populations in the solar neighborhood. Evidence from stellar abundance ratios and kinematics. *A&A* 511, L10. doi:10.1051/0004-6361/200913877. 1002.4514.
- Noguchi M (1998), Mar. Clumpy star-forming regions as the origin of the peculiar morphology of high-redshift galaxies. *Nature* 392 (6673): 253–256. doi:10.1038/32596.
- Noguchi M (2018), Jul. The formation of solar-neighbourhood stars in two generations separated by 5 billion years. *Nature* 559 (7715): 585–588. doi:10.1038/s41586-018-0329-2. 1809.02299.
- Okalidis P, Grand RJJ, Yates RM and Springel V (2022), Aug. Stellar migration in the Auriga simulations. *MNRAS* 514 (4): 5085–5104. doi:10.1093/mnras/stac1635. 2206.05304.
- Pérez-Villegas A, Portail M, Wegg C and Gerhard O (2017), May. Revisiting the Tale of Hercules: How Stars Orbiting the Lagrange Points Visit the Sun. *ApJL* 840 (1), L2. doi:10.3847/2041-8213/aa6c26. 1702.06541.
- Peters W. L. I (1975), Feb. Models for the inner regions of the Galaxy. I. An elliptical streamline model. *ApJ* 195: 617–629. doi:10.1086/153363.
- Poggio E, Drimmel R, Andrae R, Bailer-Jones CAL, Fouesneau M, Lattanzi MG, Smart RL and Spagna A (2020), Mar. Evidence of a dynamically evolving Galactic warp. *Nature Astronomy* 4: 590–596. doi:10.1038/s41550-020-1017-3. 1912.10471.
- Poggio E, Drimmel R, Cantat-Gaudin T, Ramos P, Ripepi V, Zari E, Andrae R, Blomme R, Chemin L, Clementini G, Figueras F, Fouesneau M, Frémat Y, Lobel A, Marshall DJ, Muraveva T and Romero-Gómez M (2021), Jul. Galactic spiral structure revealed by Gaia EDR3. *A&A* 651, A104. doi:10.1051/0004-6361/202140687. 2103.01970.
- Poggio E, Khanna S, Drimmel R, Zari E, D’Onghia E, Lattanzi MG, Palicio PA, Recio-Blanco A and Thulasidharan L (2024), Jul. The Great Wave: Evidence of a large-scale vertical corrugation propagating outwards in the Galactic disc. *arXiv e-prints*, arXiv:2407.18659doi:10.48550/arXiv.2407.18659. 2407.18659.
- Queiroz ABA, Chiappini C, Pérez-Villegas A, Khalatyan A, Anders F, Barbuy B, Santiago BX, Steinmetz M, Cunha K, Schultheis M, Majewski SR, Minchev I, Minniti D, Beaton RL, Cohen RE, da Costa LN, Fernández-Trincado JG, García-Hernández DA, Geisler D, Hasselquist S, Lane RR, Nitschelm C, Rojas-Arriagada A, Roman-Lopes A, Smith V and Zasowski G (2021), Dec. The Milky Way bar and bulge revealed by APOGEE and Gaia EDR3. *A&A* 656, A156. doi:10.1051/0004-6361/202039030. 2007.12915.
- Queiroz ABA, Anders F, Chiappini C, Khalatyan A, Santiago BX, Nepal S, Steinmetz M, Gallart C, Valentini M, Dal Ponte M, Barbuy B, Pérez-

- Villegas A, Masseron T, Fernández-Trincado JG, Khoperskov S, Minchev I, Fernández-Alvar E, Lane RR and Nitschelm C (2023), May. StarHorse results for spectroscopic surveys and Gaia DR3: Chrono-chemical populations in the solar vicinity, the genuine thick disk, and young alpha-rich stars. *A&A* 673, A155. doi:10.1051/0004-6361/202245399. 2303.09926.
- Rahimi A, Carrell K and Kawata D (2014), Nov. Numerical simulation of a possible origin of the positive radial metallicity gradient of the thick disk. *Research in Astronomy and Astrophysics* 14 (11), 1406–1414. doi:10.1088/1674-4527/14/11/004. 1308.2061.
- Read JI (2014), Jun. The local dark matter density. *Journal of Physics G Nuclear Physics* 41 (6), 063101. doi:10.1088/0954-3899/41/6/063101. 1404.1938.
- Reid MJ and Brunthaler A (2020), Mar. The Proper Motion of Sagittarius A*. III. The Case for a Supermassive Black Hole. *ApJ* 892 (1), 39. doi:10.3847/1538-4357/ab76cd. 2001.04386.
- Reid MJ, Menten KM, Brunthaler A, Zheng XW, Dame TM, Xu Y, Li J, Sakai N, Wu Y, Immer K, Zhang B, Sanna A, Moscadelli L, Rygl KJL, Bartkiewicz A, Hu B, Quiroga-Núñez LH and van Langevelde HJ (2019), Nov. Trigonometric Parallaxes of High-mass Star-forming Regions: Our View of the Milky Way. *ApJ* 885 (2), 131. doi:10.3847/1538-4357/ab4a11. 1910.03357.
- Rix HW, Chandra V, Andrae R, Price-Whelan AM, Weinberg DH, Conroy C, Fouesneau M, Hogg DW, De Angeli F, Naidu RP, Xiang M and Ruz-Mieres D (2022), Dec. The Poor Old Heart of the Milky Way. *ApJ* 941 (1), 45. doi:10.3847/1538-4357/ac9e01. 2209.02722.
- Robertson B, Bullock JS, Cox TJ, Di Matteo T, Hernquist L, Springel V and Yoshida N (2006), Jul. A Merger-driven Scenario for Cosmological Disk Galaxy Formation. *ApJ* 645 (2): 986–1000. doi:10.1086/504412. astro-ph/0503369.
- Robin AC, Reylé C, Derrière S and Picaud S (2003), Oct. A synthetic view on structure and evolution of the Milky Way. *A&A* 409: 523–540. doi:10.1051/0004-6361:20031117.
- Robin AC, Bienaymé O, Salomon JB, Reylé C, Lagarde N, Figueras F, Mor R, Fernández-Trincado JG and Montillaud J (2022), Nov. A self-consistent dynamical model of the Milky Way disc adjusted to Gaia data. *A&A* 667, A98. doi:10.1051/0004-6361/202243686. 2208.13827.
- Sanders JL, Smith L and Evans NW (2019), Oct. The pattern speed of the Milky Way bar from transverse velocities. *MNRAS* 488 (4): 4552–4564. doi:10.1093/mnras/stz1827. 1903.02009.
- Sanders JL, Kawata D, Matsunaga N, Sormani MC, Smith LC, Minniti D and Gerhard O (2024), May. The epoch of the Milky Way's bar formation: dynamical modelling of Mira variables in the nuclear stellar disc. *MNRAS* 530 (3): 2972–2993. doi:10.1093/mnras/stae711. 2311.00035.
- Schönrich R and Binney J (2009), Jun. Chemical evolution with radial mixing. *MNRAS* 396 (1): 203–222. doi:10.1111/j.1365-2966.2009.14750.x. 0809.3006.
- Schönrich R and Dehnen W (2018), Aug. Warp, waves, and wrinkles in the Milky Way. *MNRAS* 478 (3): 3809–3824. doi:10.1093/mnras/sty1256. 1712.06616.
- Sellwood JA (2011), Jan. The lifetimes of spiral patterns in disc galaxies. *MNRAS* 410 (3): 1637–1646. doi:10.1111/j.1365-2966.2010.17545.x. 1008.2737.
- Sellwood JA and Binney JJ (2002), Nov. Radial mixing in galactic discs. *MNRAS* 336 (3): 785–796. doi:10.1046/j.1365-8711.2002.05806.x. astro-ph/0203510.
- Shen J, Rich RM, Kormendy J, Howard CD, De Propris R and Kunder A (2010), Sep. Our Milky Way as a Pure-disk Galaxy—A Challenge for Galaxy Formation. *ApJL* 720 (1): L72–L76. doi:10.1088/2041-8205/720/1/L72. 1005.0385.
- Skowron DM, Skowron J, Mróz P, Udalski A, Pietrukowicz P, Soszyński I, Szymański MK, Poleski R, Kozłowski S, Ulaczyk K, Rybicki K and Iwanek P (2019), Aug. A three-dimensional map of the Milky Way using classical Cepheid variable stars. *Science* 365 (6452): 478–482. doi:10.1126/science.aau3181. 1806.10653.
- Sofue Y (2020), Apr. Rotation Curve of the Milky Way and the Dark Matter Density. *Galaxies* 8 (2), 37. doi:10.3390/galaxies8020037. 2004.11688.
- Sormani MC, Binney J and Magorrian J (2015), Dec. Gas flow in barred potentials - III. Effects of varying the quadrupole. *MNRAS* 454 (2): 1818–1839. doi:10.1093/mnras/stv2067. 1507.03078.
- Sun W, Huang Y, Shen H, Wang C, Zhang H, Tian Z, Liu X and Jiang B (2024), Jan. Mapping the Galactic Disk with the LAMOST and Gaia Red Clump Sample. VIII. Mapping the Kinematics of the Galactic Disk Using Mono-age and Mono-abundance Stellar Populations. *ApJ* 961 (1), 141. doi:10.3847/1538-4357/ad06ad. 2310.15408.
- Tremaine S, Frankel N and Bovy J (2023), May. The origin and fate of the Gaia phase-space snail. *MNRAS* 521 (1): 114–123. doi:10.1093/mnras/stad577. 2212.11990.
- Tsujiimoto T and Baba J (2020), Dec. Remarkable Migration of the Solar System from the Innermost Galactic Disk; a Wander, a Wobble, and a Climate Catastrophe on the Earth. *ApJ* 904 (2), 137. doi:10.3847/1538-4357/abc00a. 2010.05962.
- Vallée JP (2021), Sep. A low density wave's spiral pattern speed, from the tracer separations (age gradient) across a spiral arm in the Milky Way. *MNRAS* 506 (1): 523–530. doi:10.1093/mnras/stab1679. 2106.15761.
- Vislosky E, Minchev I, Khoperskov S, Martig M, Buck T, Hilmi T, Ratcliffe B, Bland-Hawthorn J, Quillen AC, Steinmetz M and de Jong R (2024), Feb. Gaia DR3 data consistent with a short bar connected to a spiral arm. *MNRAS* 528 (2): 3576–3591. doi:10.1093/mnras/stae083. 2312.03854.
- Wang W, Han J, Cautun M, Li Z and Ishigaki MN (2020), May. The mass of our Milky Way. *Science China Physics, Mechanics, and Astronomy* 63 (10), 109801. doi:10.1007/s11433-019-1541-6. 1912.02599.
- Wang HF, Chrobáková Ž, López-Corredoira M and Sylos Labini F (2023), Jan. Mapping the Milky Way Disk with Gaia DR3: 3D Extended Kinematic Maps and Rotation Curve to ≈ 30 kpc. *ApJ* 942 (1), 12. doi:10.3847/1538-4357/aca27c. 2211.05668.
- Wegg C and Gerhard O (2013), Nov. Mapping the three-dimensional density of the Galactic bulge with VVV red clump stars. *MNRAS* 435 (3): 1874–1887. doi:10.1093/mnras/stt1376. 1308.0593.
- Wegg C, Gerhard O and Portail M (2015), Jul. The structure of the Milky Way's bar outside the bulge. *MNRAS* 450 (4): 4050–4069. doi:10.1093/mnras/stv745. 1504.01401.
- Wielen R, Fuchs B and Dettbarn C (1996), Oct. On the birth-place of the Sun and the places of formation of other nearby stars. *A&A* 314: 438.
- Yoshii Y (1982), Jan. Density distribution of faint stars in the direction of the north galactic pole. *PASJ* 34: 365–379.
- Zhang H and Sanders JL (2023), May. A kinematic calibration of the O-rich Mira variable period-age relation from Gaia. *MNRAS* 521 (1): 1462–1478. doi:10.1093/mnras/stad575. 2302.10024.
- Zhang H, Belokurov V, Evans NW, Kane SG and Sanders JL (2024), Sep. Kinematics and dynamics of the Galactic bar revealed by Gaia long-period variables. *MNRAS* 533 (3): 3395–3414. doi:10.1093/mnras/stae2023. 2406.06678.